JCB Journal of Cell Biology

ARTICLE

Src activation by Chk1 promotes actin patch formation and prevents chromatin bridge breakage in cytokinesis

Maria Dandoulaki[1], Eleni Petsalaki[1], David Sumpton[2], Sara Zanivan[2,3], and George Zachos[1]

In cytokinesis with chromatin bridges, cells delay abscission and retain actin patches at the intercellular canal to prevent chromosome breakage. In this study, we show that inhibition of Src, a protein-tyrosine kinase that regulates actin dynamics, or Chk1 kinase correlates with chromatin breakage and impaired formation of actin patches but not with abscission in the presence of chromatin bridges. Chk1 is required for optimal localization and complete activation of Src. Furthermore, Chk1 phosphorylates human Src at serine 51, and phosphorylated Src localizes to actin patches, the cell membrane, or the nucleus. Nonphosphorylatable mutation of S51 to alanine reduces Src catalytic activity and impairs formation of actin patches, whereas expression of a phosphomimicking Src-S51D protein rescues actin patches and prevents chromatin breakage in Chk1-deficient cells. We propose that Chk1 phosphorylates Src-S51 to fully induce Src kinase activity and that phosphorylated Src promotes formation of actin patches and stabilizes chromatin bridges. These results identify proteins that regulate formation of actin patches in cytokinesis.

Introduction

Chromatin bridges are strands of incompletely segregated chromatin that connect anaphase poles or daughter nuclei and have been linked to tumorigenesis (Hoffelder et al., 2004; Ganem and Pellman, 2012). In the presence of chromatin bridges, eukaryotic cells delay abscission, the final cut of the narrow cytoplasmic canal that connects the daughter cells, to prevent tetraploidization by regression of the cleavage furrow or chromatin breakage (Steigemann et al., 2009; Nähse et al., 2017). In mammals, this abscission delay is called the abscission checkpoint and relies on the Aurora B protein kinase (Steigemann et al., 2009; Nähse et al., 2017). Activated Aurora B phosphorylates the endosomal sorting complex required for transport-III (ESCRT-III) subunit charged multivesicular body protein 4C (Chmp4c; Capalbo et al., 2012; Carlton et al., 2012; Petsalaki and Zachos, 2016). In turn, phosphorylated Chmp4c can cooperate with several proteins to inhibit the ATPase Vps4 at the midbody and prevent its activity on ESCRT-III filaments in order to inhibit abscission (Morita et al., 2007; Thoresen et al., 2014; Caballe et al., 2015). Furthermore, cells with chromatin bridges form and retain actin-rich structures called actin patches at the base of the chromatin bridge (Chen and Doxsey, 2009; Steigemann et al., 2009). It is suggested that actin patches stabilize the intercellular canal until the DNA bridge is resolved; however, how actin patches are formed has not been previously reported.

Src is a nonreceptor tyrosine kinase that is involved in a diverse spectrum of biological activities including cell proliferation, adhesion, spreading, and migration (Playford and Schaller, 2004). Src is located at the plasma membrane and is also found at late endosomes, the Golgi apparatus, and the nucleus (Takahashi et al., 2009). Src family kinases share a conserved domain structure consisting of an amino-terminal membrane-binding SH4 domain with a myristoylation sequence, followed by a "Unique" region that is divergent among family members (amino acids 20–85 of human Src), consecutive Src homology 3 (SH3) and SH2 domains, and a kinase domain that is followed by a short C-terminal tail (Maffei et al., 2015; Roskoski, 2015). The C-terminal tail contains an autoinhibitory phosphorylation site (tyrosine 530 [Y530] in human Src), and phosphorylation at this site promotes assembly of the SH2, SH3, and kinase domains into an autoinhibited "closed" conformation (Xu et al., 1997; Brábek et al., 2002). Displacement of the SH3- and SH2-mediated intramolecular interactions by Src binding to downstream substrates or higher-affinity ligands allows dephosphorylation of Src-Y530, followed by autophosphorylation of tyrosine 419 (Y419)

[1]Department of Biology, University of Crete, Heraklion, Greece; [2]Cancer Research UK Beatson Institute, Glasgow, Scotland, UK; [3]Institute of Cancer Sciences, Wolfson Wohl Cancer Research Centre, University of Glasgow, Glasgow, Scotland, UK.

Correspondence to George Zachos: gzachos@uoc.gr.

© 2018 Dandoulaki et al. This article is distributed under the terms of an Attribution–Noncommercial–Share Alike–No Mirror Sites license for the first six months after the publication date (see http://www.rupress.org/terms/). After six months it is available under a Creative Commons License (Attribution–Noncommercial–Share Alike 4.0 International license, as described at https://creativecommons.org/licenses/by-nc-sa/4.0/).

Downloaded from http://rupress.org/jcb/article-pdf/217/9/3071/1614074/jcb_201802102.pdf by guest on 08 February 2026

Check for updates

https://doi.org/10.1083/jcb.201802102

inside the human Src catalytic loop, and leading to conversion of the enzyme into an active "open" form (Bernadó et al., 2008; Roskoski, 2015). In addition, the Unique domain of Src contains phosphorylation residues that activate Src by promoting dephosphorylation of the autoinhibitory site (Shenoy et al., 1992; Stover et al., 1994) or regulate Src binding to lipids (Pérez et al., 2013; Amata et al., 2014).

Activating mutations in cellular Src or infection with the Src encoding Rous sarcoma virus can cause oncogenic transformation that is accompanied by dramatic changes in the actin cytoskeleton (Frame, 2002). Src binds to FAK at focal adhesions and phosphorylates FAK at various residues including tyrosine 925 (Y925) to activate FAK or create binding sites for adaptor proteins (Brunton et al., 2005; Mitra et al., 2005). In turn, the FAK–Src signaling complex promotes changes in actin cytoskeleton and regulates focal adhesion turnover (Goldberg et al., 2003; Brown et al., 2005; Mitra et al., 2005). Src phosphorylates cortactin to enhance actin nucleation and binds to formins to induce formation of stress fibers (Tominaga et al., 2000; Tehrani et al., 2007). In addition, Src signaling is involved in the completion of cytokinesis (Kasahara et al., 2007a; Kamranvar et al., 2016).

Chk1 kinase was first identified to regulate the DNA damage response (Smith et al., 2010); however, it is also required for proper mitotic cell division (Zachos et al., 2007; Peddibhotla et al., 2009). Chk1 phosphorylates the mitotic kinase Aurora B in prometaphase and metaphase to induce Aurora B catalytic activity and promote correction of misattached kinetochore–microtubules (Petsalaki et al., 2011; Petsalaki and Zachos, 2013). Also, Chk1 is required for successful chromosome segregation and cytokinesis and for an abscission delay in response to replication stress (Peddibhotla et al., 2009; Petsalaki et al., 2014; Mackay and Ullman, 2015). In this study, we show that Chk1 phosphorylates human Src at the newly identified site serine 51 to fully induce Src kinase activity. We also show that phosphorylated Src promotes formation of actin patches and prevents chromosome breakage in cytokinesis with chromatin bridges.

Results

Src and Chk1 prevent chromatin breakage in cytokinesis

Because Src and Chk1 are involved in completion of cytokinesis (Kasahara et al., 2007a; Mackay and Ullman, 2015), we investigated their potential role in cytokinesis with chromatin bridges. Confocal microscopy analysis of fixed human colon carcinoma BE cells in telophase showed that 30–34% cells treated with PP2, a catalytic inhibitor of Src family tyrosine kinases, or depleted of Chk1 or Src by, respectively, Chk1 siRNA (siChk1) or Src siRNA (siSrc), exhibited broken DNA bridges compared with ∼5% control (Fig. 1, A and B; and Fig. S1, A and B). Treatment with PP2 did not exacerbate chromatin breakage in Chk1-depleted cells, suggesting that Chk1 and Src prevent chromatin breakage by acting through the same mechanism (Fig. 1 B). Also, Chk1 or Src inhibition increased the frequency of chromatin bridges that were positive for phospho-Ser139 histone H2A.X (γ-H2AX) staining, which is a marker for double-strand DNA breaks (Fig. 1, C and D; Janssen et al., 2011).

To further investigate the role of Chk1 and Src in chromatin breakage, HeLa cells expressing the inner nuclear envelope marker LAP2b fused to RFP (LAP2b-RFP) and displaying LAP2b-RFP bridges in cytokinesis were monitored for up to 180 min by time-lapse microscopy. LAP2b-RFP localizes around chromatin from late anaphase and correlates with chromatin bridges (Steigemann et al., 2009). We found that 15/15 control cells exhibiting intercellular canals with LAP2b-RFP bridges sustained those canals for the duration of the experiment (Fig. 1 E, Fig. S1 C, and Video 1). In contrast, 11/13 cells treated with PP2 exhibited breakage of intercellular canals containing LAP2b-RFP bridges after 47 ± 14 min (n = 11; Fig. 1 E, Fig. S1 C, and Video 2). Furthermore, 11/13 cells treated with the selective Chk1 inhibitor UCN-01 displaying intercellular canals with LAP2b-RFP bridges exhibited breakage of those canals after 52 ± 15 min (n = 11; Fig. 1 E, Fig. S1 C, and Video 3). Confocal microscopy analysis of fixed HeLa LAP2b-RFP cells also showed that Chk1- or Src-deficient cells exhibited increased frequency of broken LAP2b-RFP bridges compared with controls (Fig. 1, F and G). These results suggest that Chk1 and Src prevent chromatin breakage in cytokinesis with chromatin bridges.

Fragmented chromatin bridges can lead to the formation of micronuclei and accumulation of DNA damage (Hoffelder et al., 2004). Depletion of Src or Chk1 increased the frequency of BE cells exhibiting micronuclei that were devoid of nuclear lamin B2 compared with controls (Fig. 2, A and C), which is consistent with these micronuclei being bridge-derived (Utani et al., 2010). Furthermore, Src- or Chk1-deficient cells exhibited increased frequency of micronuclei that were positive for γ-H2AX staining compared with controls (Fig. 2, B and C). These results suggest that Src and Chk1 are required to prevent formation of micronuclei and generation of DNA damage in cytokinesis with chromatin bridges.

Src and Chk1 are required for actin patch formation in cytokinesis with chromatin bridges

Control cells with chromatin bridges exhibited actin patches, i.e., regions of relatively high intensity F-actin staining, at both sides of the DNA bridge (Fig. 2 D). However, Src- or Chk1-deficient cells exhibited reduced actin patches, and this was not a result of diminished total levels of actin compared with controls (Fig. 2, D–F; and Fig. S1 D). Control cells with relatively strong or weak DNA bridge labeling (i.e., with DNA bridge fluorescence above or below, respectively, the control mean) exhibited similar actin patches (Fig. 3, A and B). Also, Chk1- or Src-depleted cells exhibited reduced actin patches compared with controls regardless of the intensity of the DNA bridge signal (relatively strong versus weak signal; Fig. 3, A and B; and Fig. S1 E), suggesting that the amount of DNA inside the intercellular canal does not associate with the intensity of actin patches. Actin patches were also diminished in Src- or Chk1-deficient cells with intact DNA bridges, suggesting that impaired actin patches were not a consequence of chromatin breakage (Fig. S1, F–H). Expression of WT GFP-Src that is resistant to degradation by a second siSrc (siSrc-2), or GFP-Chk1, resistant to degradation by siChk1-2, reduced chromatin breakage and rescued formation of actin patches after depletion of the endogenous Src or Chk1 compared with

Downloaded from http://rupress.org/jcb/article-pdf/217/9/3071/1614074/jcb_201802102.pdf by guest on 08 February 2026

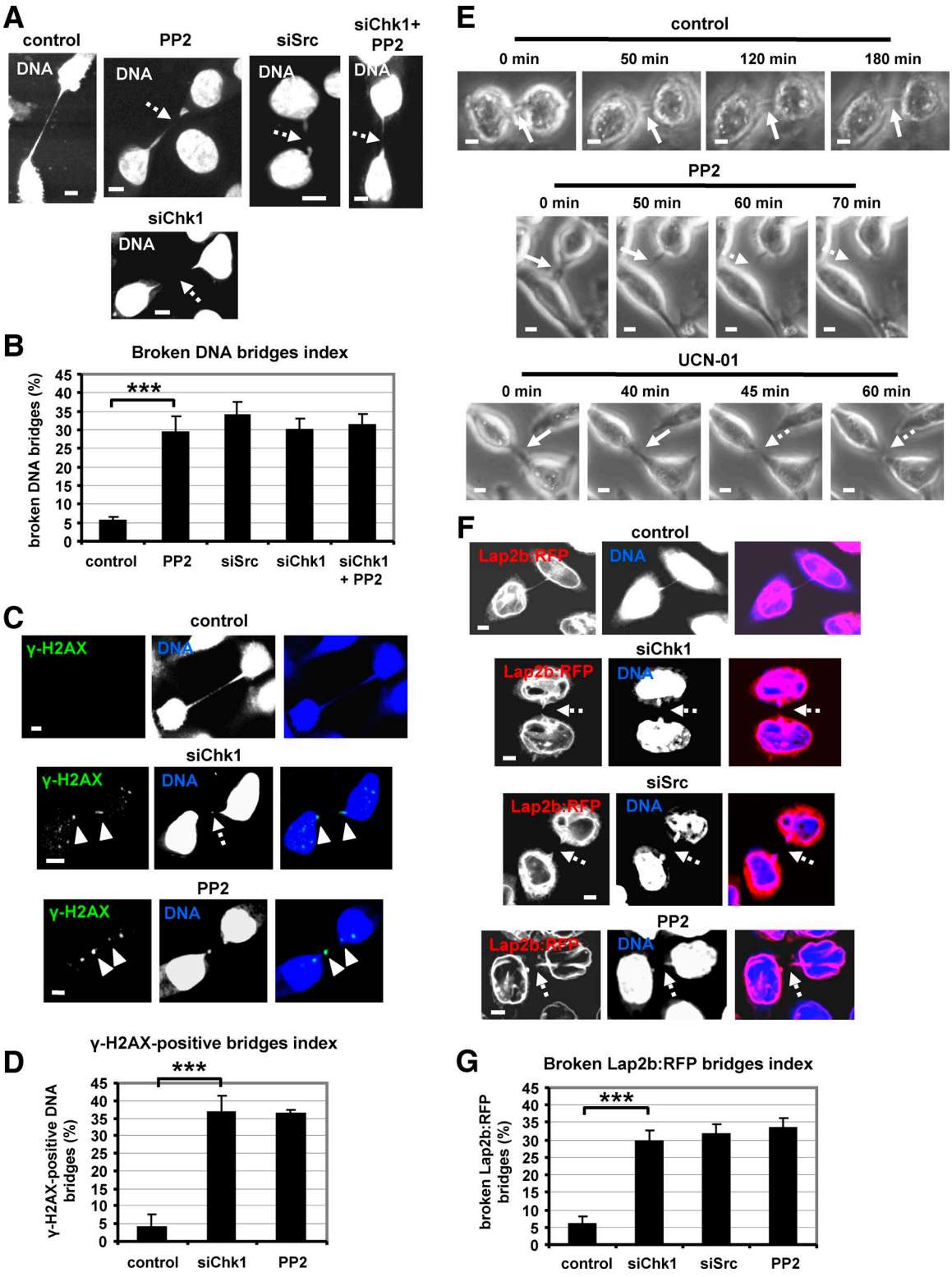

Figure 1. **Src or Chk1-inhibition correlates with chromatin breakage. (A)** DNA bridges in cells transfected with negative siRNA (control), siSrc, or siChk1, or treated with PP2 for 5 h. **(B)** Percentage of DNA bridges that appear broken. **(C and D)** γ-H2AX staining (C) and frequency of telophase cells with DNA bridges exhibiting γ-H2AX staining (D). Arrowheads indicate γ-H2AX foci on DNA bridges. **(E and F)** HeLa cells expressing LAP2b-RFP were analyzed by phase-contrast live-cell imaging (E) or by fluorescence microscopy of fixed samples (F). Time is from the detection of the intercellular canals containing LAP2b-RFP bridges. Intact intercellular canals are indicated by solid arrows, and broken canals are indicated by dotted arrows. Related to Videos 1, 2, and 3. **(G)** Percentage of LAP2b-RFP–positive bridges that appear broken. Broken DNA or LAP2b bridges are indicated by dotted arrows. Error bars show the SD from the mean from three independent experiments. A minimum of 50 fixed cells with chromatin bridges was analyzed per experiment. ***, $P < 0.001$ compared with the control. Statistically significant differences were determined by ANOVA and Student's *t* test. Bars, 5 µm.

Downloaded from http://rupress.org/jcb/article-pdf/217/9/3071/1614074/jcb_201802102.pdf by guest on 08 February 2026

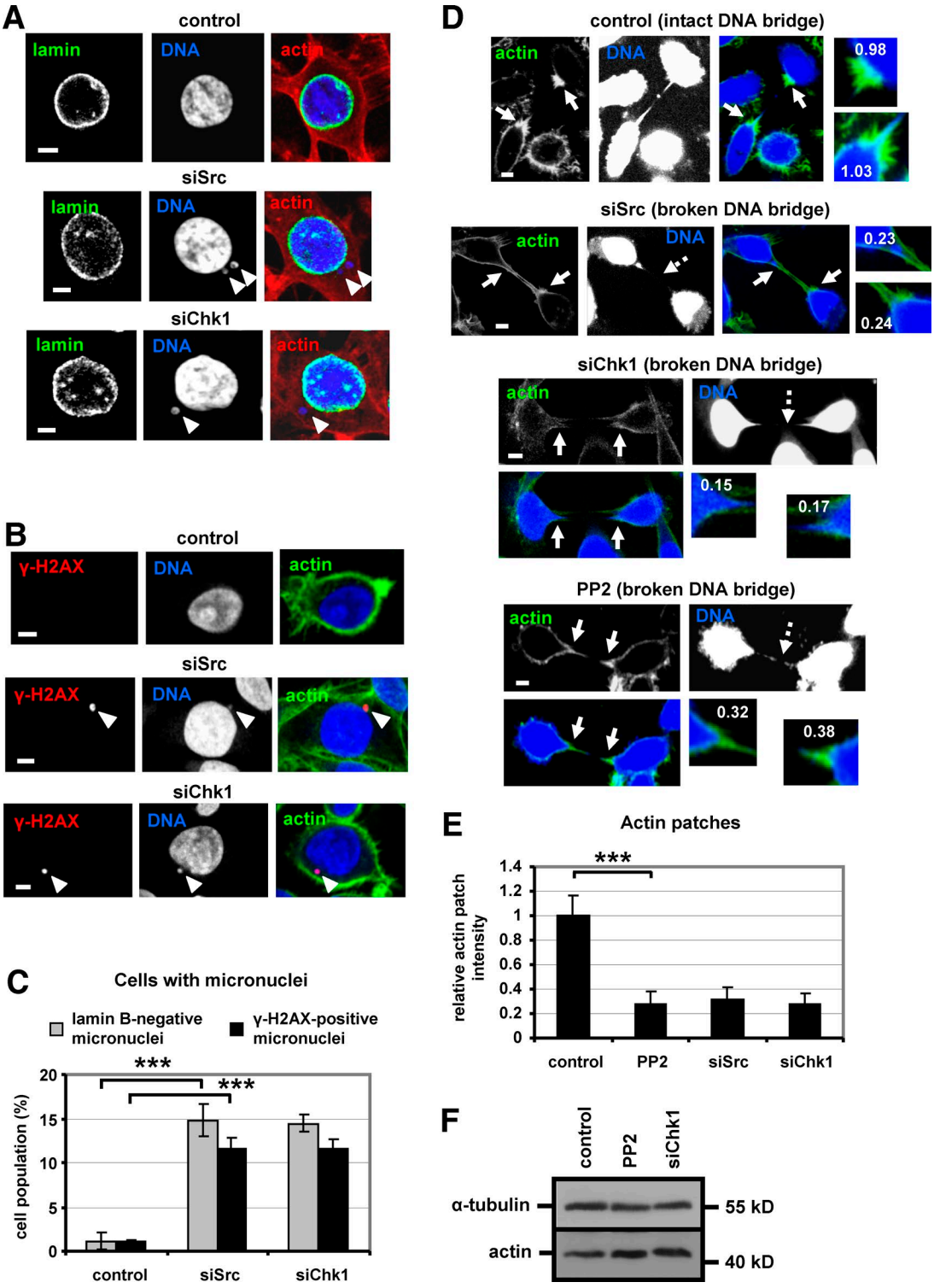

Figure 2. **Inhibition of Src or Chk1 diminishes formation of actin patches. (A and B)** Cells were transfected with negative siRNA (control), siSrc, or siChk1. Lamin B–negative (A) or γ-H2AX–positive micronuclei (B) are indicated by arrowheads. **(C)** Frequency of cells exhibiting lamin B-negative or γ-H2AX–positive micronuclei. Error bars show the SD from the mean from three independent experiments. A minimum of 150 cells was analyzed per experiment. **(D)** Cells were transfected as in A or treated with PP2 for 5 h. Broken DNA bridges are indicated by dotted arrows, and the bases of the intercellular canals are indicated by solid arrows. Relative actin patch intensity values are shown. Insets show 3× magnification of the canals bases. Bars, 5 µm. **(E)** Actin patches intensity. Relative green fluorescence intensity from D is shown, and values in control were set to 1. Error bars show the SD from the mean. $n = 30$ cells from three independent experiments. ***, $P < 0.001$ compared with the control. Statistically significant differences were determined by ANOVA and Student's t test. **(F)** Western blot analysis of total α-tubulin and actin.

Downloaded from http://rupress.org/jcb/article-pdf/217/9/3071/1614074/jcb_201802102.pdf by guest on 08 February 2026

cells expressing GFP alone (Fig. 3, C–F; and Fig. S1, I and J). These results show that Src and Chk1 are required for stable chromatin bridges and formation of actin patches in cytokinesis.

Chromatin breakage in Src- or Chk1-deficient cells is not caused by abscission

Approximately 70% of Src- or Chk1-depleted cells with broken DNA bridges exhibited intact intercellular canals as evidenced by staining with FM 1-43FX, a fluorescence lipophilic dye that labels membranes (Fig. 4, A and B; Fuenzalida et al., 2011), suggesting that chromatin breakage in Src- or Chk1-deficient cells does not correlate with abscission. For comparison, 45/45 cells treated with the Cdc-like kinase inhibitor TG003 that inhibits the abscission checkpoint (Petsalaki and Zachos, 2016) with broken DNA bridges exhibited broken intercellular canals, indicating that TG003-treated cells had finished abscission (Fig. 4, A and B). Also for comparison, 21/21 control cells with intact DNA bridges exhibited intact intercellular canals (Fig. 4 C). To further investigate the mechanism of chromatin breakage, cells expressing mutant Vps4 protein fused to GFP in which Vps4-lysine 173 was changed to glutamine (GFP-Vps4-K173Q), to abrogate ATP binding to Vps4 and inhibit abscission (Morita et al., 2007; Petsalaki and Zachos, 2016), or GFP alone were examined. In cells depleted of Src or Chk1, expression of GFP–Vps4-K173Q did not prevent breakage of DNA bridges compared with cells expressing GFP (Fig. 4, D and E). For comparison, expression of GFP-Vps4-K173Q prevented chromatin breakage after treatment with TG003 or Aurora B depletion compared with cells expressing GFP only (Fig. 4, D and E; and Fig. S2 A), confirming that Vps4-K173Q inhibits abscission under the experimental conditions used in our study (Steigemann et al., 2009; Petsalaki and Zachos, 2016). These results show that chromatin breakage in Src- or Chk1-deficient cells is not caused by abscission.

Chk1/Src and Aurora B cooperate to prevent chromatin breakage

Aurora B–deficient cells exhibit premature abscission (Steigemann et al., 2009), and Aurora B–deficient cells exhibited increased frequency of broken chromatin bridges compared with controls despite having similar actin patches (Fig. 5, A–C). Simultaneous depletion of Chk1 or Src and Aurora B exacerbated chromatin breakage, and this correlated with reduced formation of actin patches and with increased frequency of cells with broken DNA bridges with an intact midbody (i.e., without abscission) compared with cells depleted of Aurora B only (Fig. 5, A–D). The remaining double-depleted cells with broken DNA bridges exhibited midbody remnants, i.e., midbodies severed from one daughter cell or completely disassembled midbody microtubules (Fig. 5 A). Control cells with intact DNA bridges also exhibited disassembled midbody microtubules (midbody remnants) despite the abscission delay (Fig. 5 A), in agreement with previous findings (Steigemann et al., 2009). The regulatory proteins Plk1, Mklp1, and Cep55 localize to the midbody in telophase or late cytokinesis in control cells (Mishima et al., 2002; Bastos and Barr, 2010), and Chk1 or Src depletion did not impair localization of the above proteins to the midbody compared with controls (Fig. 5, E and F; and Fig. S2, B–G). It was previously reported that pharmacological inhibition of Src resulted in reduced Plk1 and increased Cep55 at the midbody in nontransformed cells (Kamranvar et al., 2016). Perhaps the difference between our results and those from Kamranvar et al. (2016) reflects physiological differences between nontransformed and cancer cells. We propose that Chk1 and Src stabilize chromatin bridges by promoting formation of actin patches. These results also suggest that Chk1 and Src cooperate with the Aurora B–mediated abscission checkpoint to prevent chromatin breakage in cytokinesis with DNA bridges.

Src and Src-signaling proteins localize to actin patches

Proteins involved in actin remodeling can localize to actin structures. We found that the endogenous total Src, autophosphorylated Src-Y419 (active Src), and transfected WT GFP-Src localized to actin patches in control cells with chromatin bridges (Figs. 3 D and 6, A and B). Phosphorylated FAK-Y925 (a phosphorylation substrate of Src; Brunton et al., 2005) and cortactin (Tehrani et al., 2007) also localized to actin patches in control cells (Fig. 6, C and E). These results indicate that actin patch formation is regulated by Src signaling. However, Chk1 was not enriched at actin patches in control cells with chromatin bridges (Fig. 6 F), suggesting that Chk1 promotes formation of actin patches without stably localizing at the site.

Chk1 is required for optimal Src localization and kinase activity

Depletion of Chk1 or, for comparison, treatment with the Src family kinase inhibitor PP2 impaired localization of total Src and cortactin at the base of the intercellular canal and reduced phosphorylation of Src-Y419 and FAK-Y925 (which are markers of Src kinase activity) compared with control cells (Fig. 6, A–E), suggesting that Chk1 is required for optimal Src localization and kinase activity in cells with chromatin bridges. Chk1-deficient cells plated on fibronectin-coated dishes exhibited reduced levels of autophosphorylated Src-Y419 and phosphorylated FAK-Y925 by 40–60% compared with controls by Western blotting (Fig. 7, A and B). For comparison, Src inhibition by PP2 reduced phosphorylation of Src-Y419 and FAK-Y925 by ∼90% compared with controls. However, Src or FAK protein levels per se were not affected by Chk1 depletion or PP2 treatment (Fig. 7, A and B). Furthermore, Chk1-deficient interphase cells without chromatin bridges exhibited reduced levels of phosphorylated Src-Y419 and phosphorylated FAK-Y925 and diminished localization of total Src to membrane ruffles compared with controls (Fig. S3, A–E).

Inhibition of Src kinase activity reduces cell spreading and produces a more round cell morphology (Elias et al., 2010). Control or Chk1-depleted cells were trypsinized, allowed to attach on fibronectin-coated dishes in the absence or presence of PP2, and observed at various times by phase-contrast time-lapse microscopy. A relatively high percentage of Chk1-deficient or PP2-treated cells remained round and highly reflective, indicating that these cells were not able to spread properly, compared with flattened controls (Fig. 7, C and D). Also, Src kinase activity promotes migration of cells during wound healing (Di Florio et al., 2007). Depletion of Chk1 decreased wound closure of a monolayer of cells compared with controls (Fig. 7, E and F). Collectively,

Downloaded from http://rupress.org/jcb/article-pdf/217/9/3071/1614074/jcb_201802102.pdf by guest on 08 February 2026

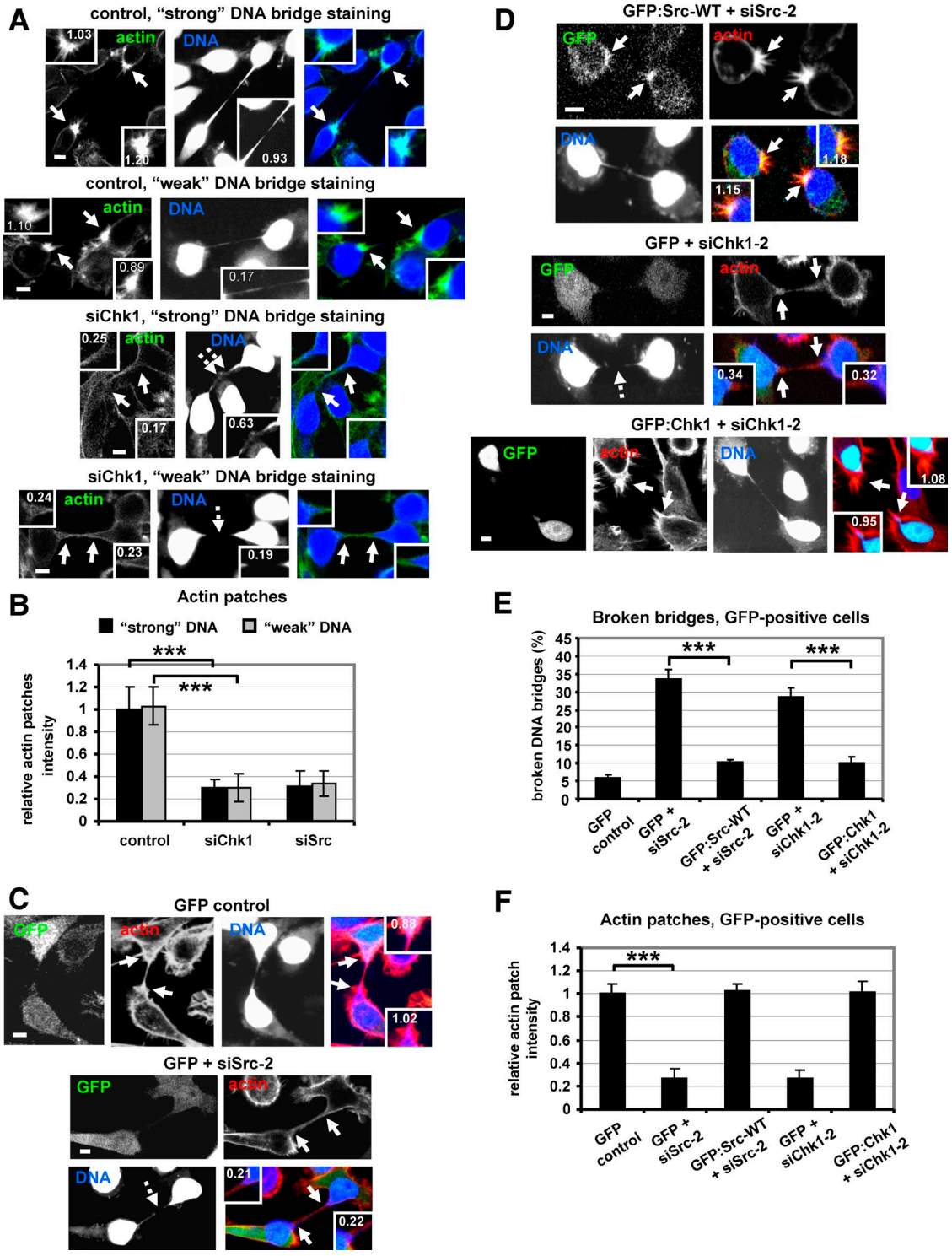

Figure 3. **Actin patches intensity is independent of the relative amount of DNA inside the intercellular canal. (A)** Actin patches in cells transfected with negative siRNA (control), siSrc, or siChk1 exhibiting relatively strong or weak DNA staining inside the intercellular canal. The mean fluorescence intensity of control DNA bridges was set to 0.5, and relative DNA intensity values are indicated in the DNA insets. Relative DNA bridge staining >0.5 was taken as strong, and DNA bridge staining <0.5 was classified as weak. **(B)** Actin patches intensity. Relative green fluorescence intensity from A is shown, and values in strong DNA control were set to 1. Error bars show the SD from the mean. *n* = 20 cells from three independent experiments. **(C and D)** Cells expressing GFP, WT GFP-Src resistant to degradation by Src-2 siRNA (siSrc-2), or GFP-Chk1 resistant to degradation by Chk1-2 siRNA (siChk1-2) were transfected with negative siRNA (control), siSrc-2, or siChk1-2. Broken DNA bridges are indicated by dotted arrows and the bases of the intercellular canals are indicated by solid arrows. Relative actin patch intensity values are shown. Insets show 1.6× magnification of the canals bases. Bars, 5 µm. **(E)** Broken bridges analysis. Error bars show the SD from the mean from three independent experiments. A minimum of 30 cells with chromatin bridges was analyzed per experiment. **(F)** Actin patches intensity. Relative red fluorescence intensity from C and D is shown, and values in GFP control were set to 1. Error bars show the SD from the mean. *n* = 30 cells from three independent experiments. ***, P < 0.001 compared with the control. Statistically significant differences were determined by ANOVA and Student's *t* test.

Downloaded from http://rupress.org/jcb/article-pdf/217/9/3071/1614074/jcb_201802102.pdf by guest on 08 February 2026

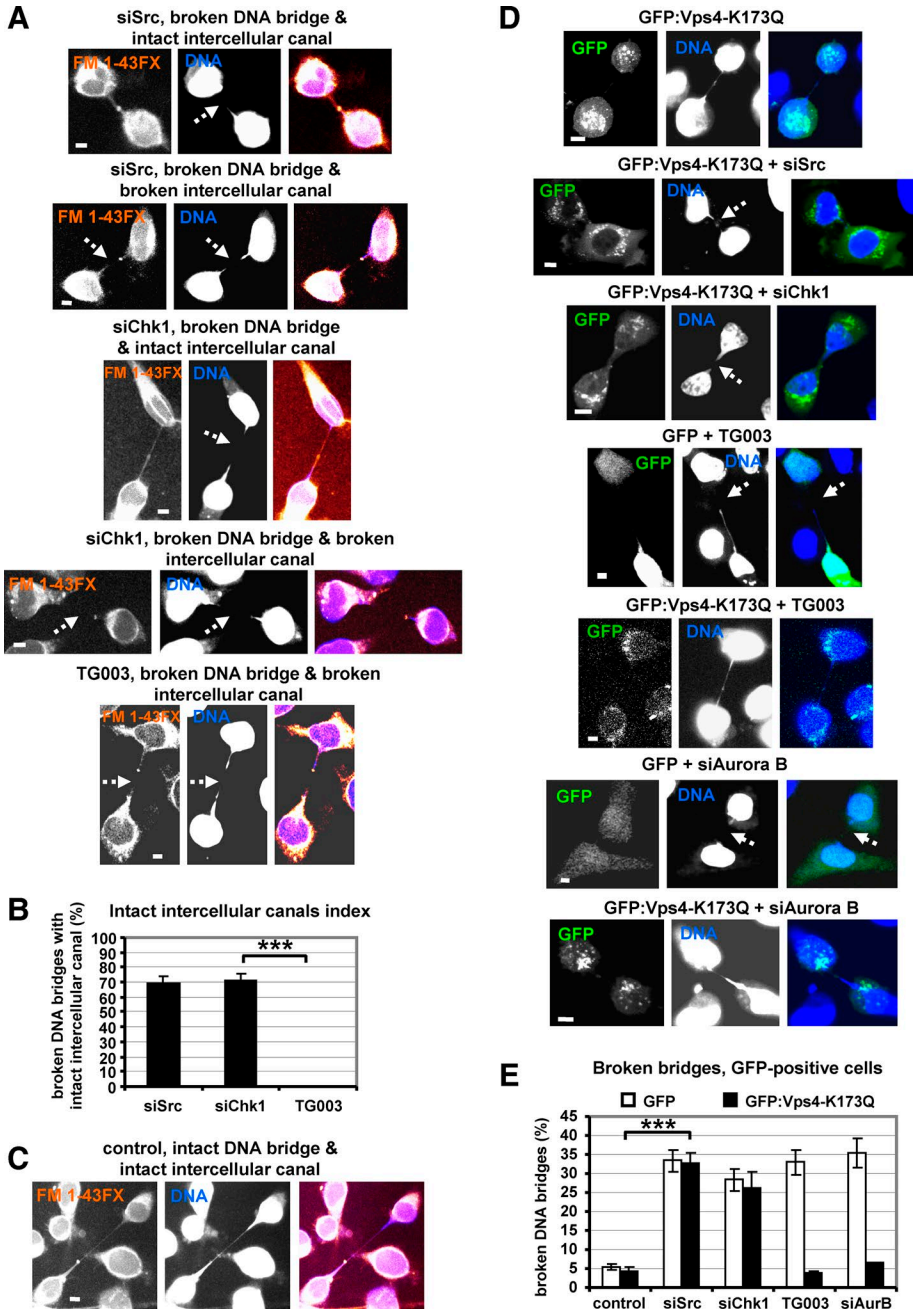

Figure 4. **Expression of dominant-negative Vps4-K173Q does not prevent chromatin breakage in Src or Chk1-deficient cells. (A and C)** Examples of cells with DNA bridges exhibiting broken or intact intercellular canals after labeling with a lipophilic dye. Cells were transfected with negative siRNA (control), siSrc, or siChk1, or treated with TG003 for 5 h and stained with FM 1-43FX. **(B)** Frequency of cells with broken DNA bridges exhibiting intact intercellular canals. Error bars show the SD from the mean from three independent experiments. 15 cells with broken chromatin bridges were analyzed per experiment. **(D)** Cells expressing GFP or GFP–Vps4-K173Q were transfected with Aurora B siRNA (siAurora B; siAurB) or treated as in A–C. Broken DNA bridges or intercellular canals are indicated by dotted arrows. Bars, 5 µm. **(E)** Percentage of DNA bridges that appear broken in GFP-positive cells. Error bars show the SD from the mean from three independent experiments. A minimum of 30 cells with chromatin bridges was analyzed per experiment. ***, $P < 0.001$ compared with the control. Statistically significant differences were determined by ANOVA and Student's *t* test.

these results show that Chk1 is required for optimal Src kinase activity in interphase cells.

Chk1 phosphorylates Src serine 51 in vitro

To investigate whether Chk1 promotes Src kinase activity through phosphorylation, avian Src fused to GST (GST-avSrc) was incubated with recombinant GST-Chk1 in kinase assays in vitro. In the presence of Chk1, GST-avSrc was radiolabeled at levels approximately sixfold higher compared with GST-avSrc alone, and this radiolabeling was reduced in the presence of the Chk1 inhibitor UCN-01, suggesting it was not a result of Src autophosphorylation (Figs. S3 F and S4, A and C). After labeling by Chk1, GST-avSrc was analyzed by liquid chromatography–mass spectrometry, and phosphorylation sites at avSrc-T46, S48, or S50, which were absent in GST-avSrc alone, were identified as Chk1 phosphorylation sites. Only monophosphorylated peptides were observed, and of these three sites, only the avSrc-S48 (Fig. S4 B) is conserved in the human protein and corresponds with human Src-S51. Nonphosphorylatable mutation of S51 to alanine (S51A) markedly reduced phosphorylation of human GST-Src (1–256) by Chk1 compared with the WT GST-Src (1–256), showing that Chk1 phosphorylates human Src at the novel site S51 in vitro (Fig. 8 A). Serine 51 is inside the Unique domain of Src and conforms to the minimum Chk1 consensus sequence R-x-x-S/T (Hutchins et al., 2000). Multiple sequence alignment demonstrated S51 is conserved in Src proteins from different species (Fig. 8 B).

Downloaded from http://rupress.org/jcb/article-pdf/217/9/3071/1614074/jcb_201802102.pdf by guest on 08 February 2026

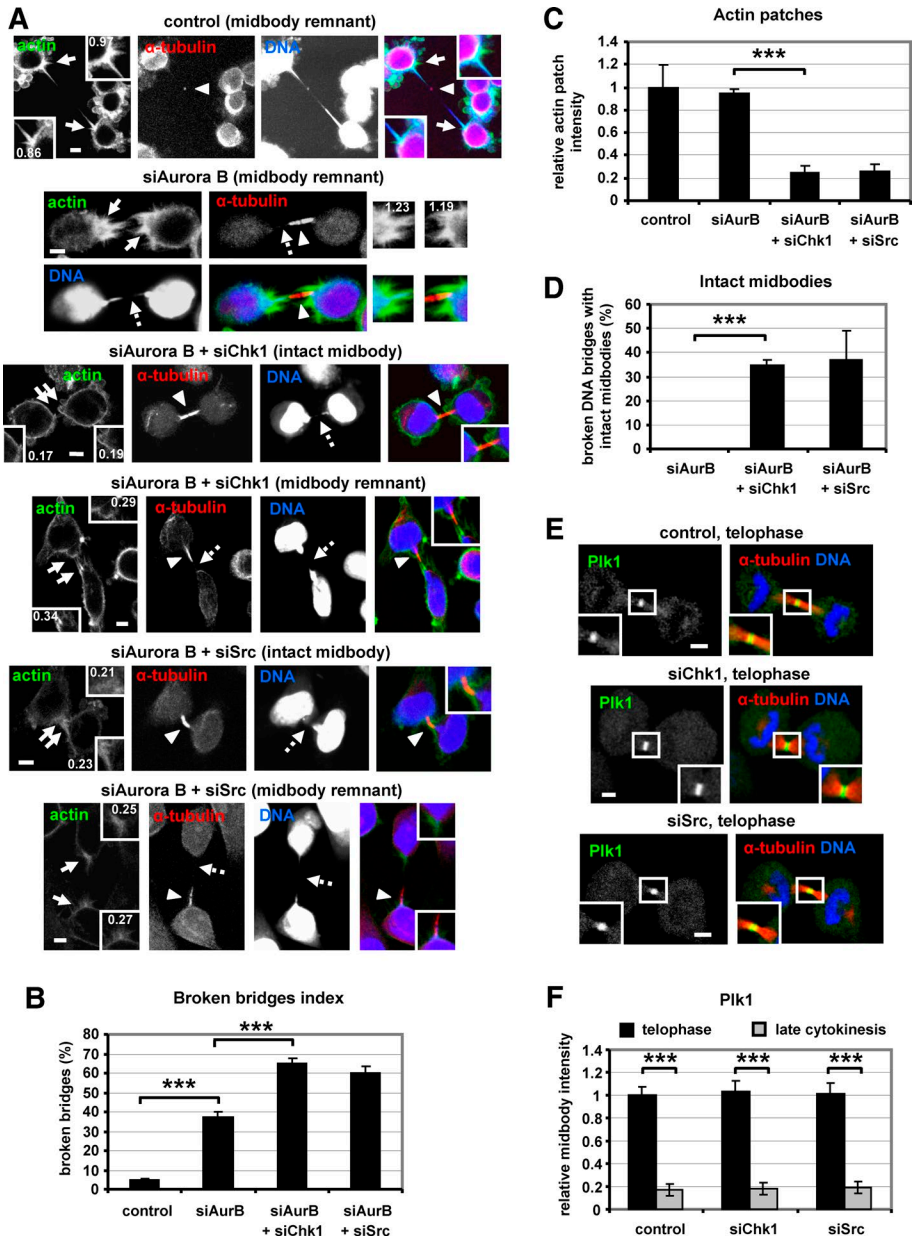

Figure 5. **Chk1 or Src depletion exacerbates chromatin breakage and reduces actin patches in Aurora B–deficient cells. (A)** Cells were transfected with negative siRNA (control), Aurora B siRNA (siAurora B), or a combination of siChk1/siSrc and siAurora B (siAurora B + siChk1; siAurora B + siSrc). Broken DNA bridges and intercellular canals are indicated by dotted arrows, midbodies and midbody remnants by arrowheads, and the bases of the intercellular canals by solid arrows. Relative actin patch intensity values are shown. Insets show 1.6× magnification of the canals bases. **(B)** Percentage of DNA bridges that appear broken. Error bars show the SD from the mean from three independent experiments. A minimum of 50 cells with chromatin bridges was analyzed per experiment. **(C)** Actin patches intensity. Relative green fluorescence from A is shown, and values in control were set to 1. Error bars show the SD from the mean. $n = 30$ from three independent experiments. **(D)** Frequency of cells with broken DNA bridges exhibiting intact midbodies. Error bars show the SD from the mean from three independent experiments. A minimum of 20 cells with chromatin bridges was analyzed per experiment. **(E)** Localization of Plk1. Insets show 1.6× magnification of the midbodies. Bars, 5 µm. **(F)** Plk1 midbody intensity. Relative green fluorescence from E is shown, and values in telophase control were set to 1. Error bars show the SD from the mean. $n = 20$ cells from two independent experiments. ***, $P < 0.001$ compared with the control. Statistically significant differences were determined by ANOVA and Student's *t* test.

Phosphorylation at S51 promotes Src kinase activity

To investigate Src-S51 phosphorylation, an antiphospho–Src-S51 antiserum was raised against the human protein sequence. This antiserum recognized phosphorylated WT GST-Src (1–256) by Chk1 but not the mutant S51A or the unphosphorylated GST-Src (1–256) protein, showing that this reagent is specific for the phosphorylation (Fig. 8 C). Recombinant GST-Chk1 enhanced Src-mediated phosphorylation of FAK-Y925 and autophosphorylation of Src-Y419, and this coincided with increased phosphorylation of Src-S51 by Chk1 in vitro (Figs. 8 D and S4 D). We propose that Chk1 phosphorylates Src-S51 and enhances Src catalytic activity in vitro.

Furthermore, WT, S51A, or S51D Src-GFP harboring a phosphomimetic mutation of S51 to aspartic acid were transfected into cells, and GFP-associated kinase activity was determined by immunoprecipitation-kinase assays by measuring phosphorylation of the FAK-Y925 substrate. GFP–Src-S51A exhibited reduced catalytic activity by ∼50% compared with the WT GFP-Src or GFP–Src-S51D (Fig. 8 E). In comparison, treatment of cells with PP2 almost completely inhibited WT Src-GFP kinase activity as measured by autophosphorylation of Src-Y419 (Fig. S4 E). In addition, immunoprecipitated S51D but not S51A or WT GFP-Src from Chk1-depleted cells phosphorylated FAK-Y925 to levels similar to WT GFP-Src from Chk1-proficient cells, showing that GFP–Src-S51D catalytic activity is independent of Chk1 (Fig. 8 F). Together, these results show that S51 phosphorylation is required for complete Src catalytic activity.

Phosphorylation at S51 enhances Src catalytic activity in the absence of Y530 phosphorylation

One possibility is that S51 phosphorylation enhances Src catalytic activity by promoting dephosphorylation of the inhibitory site Src-Y530 (Shenoy et al., 1992; Stover et al., 1994). To investigate this, we generated a mutant GFP–Src-Y530F protein

Downloaded from http://rupress.org/jcb/article-pdf/217/9/3071/1614074/jcb_201802102.pdf by guest on 08 February 2026

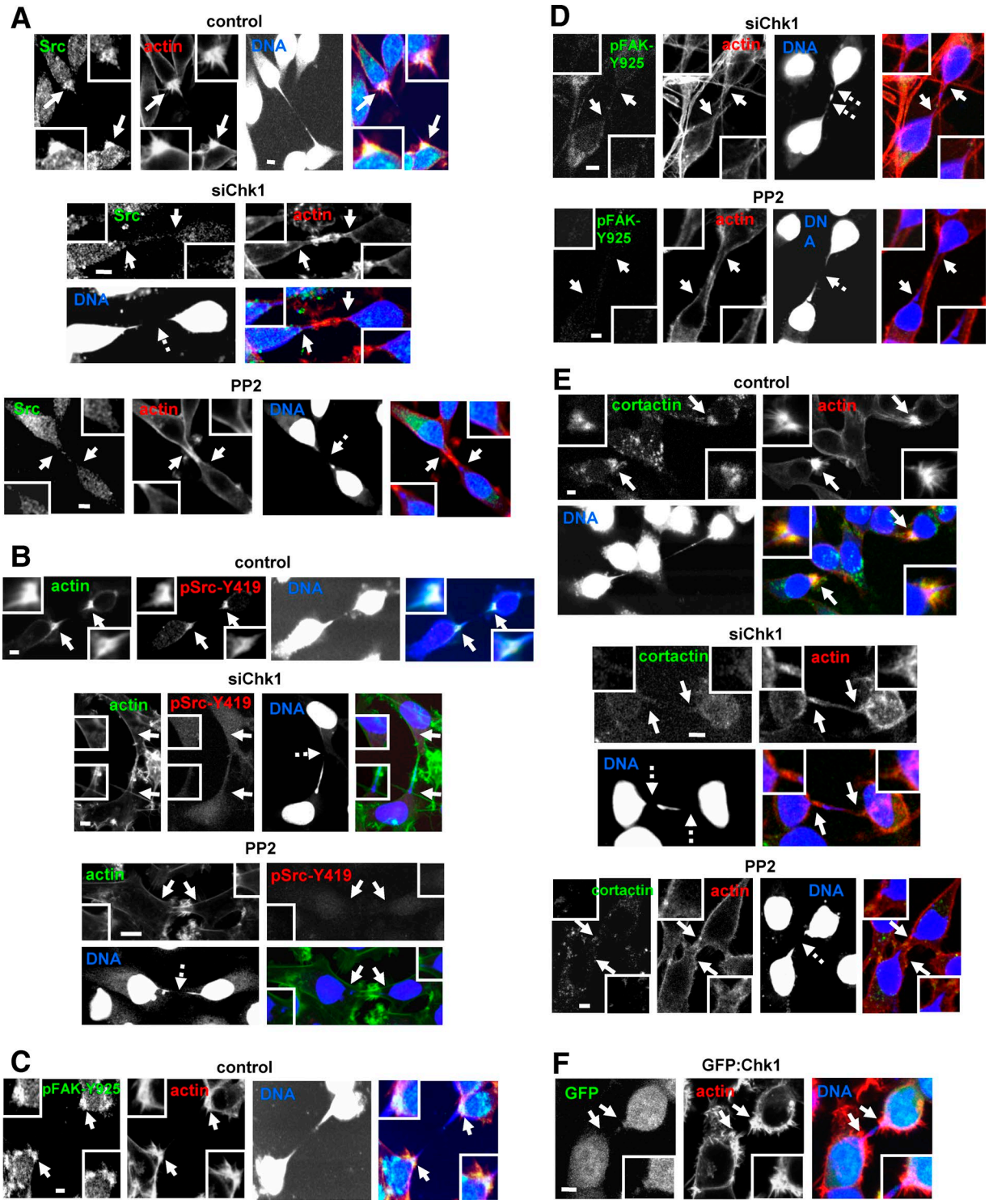

Figure 6. **Src localizes to actin patches in cells with chromatin bridges. (A–E)** Localization of Src (A), phosphorylated Src-Y419 (pSrc-Y419; B), phosphorylated FAK-Y925 (pFAK-Y925; C and D), or cortactin (E). Cells were transfected with negative siRNA (control) or siChk1, or treated with PP2 for 5 h. **(F)** Localization of GFP-Chk1. Broken DNA bridges are indicated by dotted arrows, and the bases of the intercellular canals are indicated by solid arrows. Images are representative of 20 cells from two independent experiments. Insets show 1.6× magnification of the canals bases. Bars, 5 µm.

harboring a nonphosphorylatable mutation of Y530 to phenylalanine (Y530F). GFP–Src-Y530F exhibited increased catalytic activity compared with the WT GFP-Src as evidenced by phosphorylation of FAK-Y925 substrate by the immunoprecipitated GFP proteins in vitro (Fig. 9 A), in agreement with previous findings (Piwnica-Worms et al., 1987; Brábek et al., 2002). However, introducing the S51A mutation into the activated GFP–Src-Y530F reduced its catalytic activity (Fig. 9 A), showing that S51 phosphorylation can promote Src catalytic activity in the absence of Y530 phosphorylation.

Downloaded from http://rupress.org/jcb/article-pdf/217/9/3071/1614074/jcb_201802102.pdf by guest on 08 February 2026

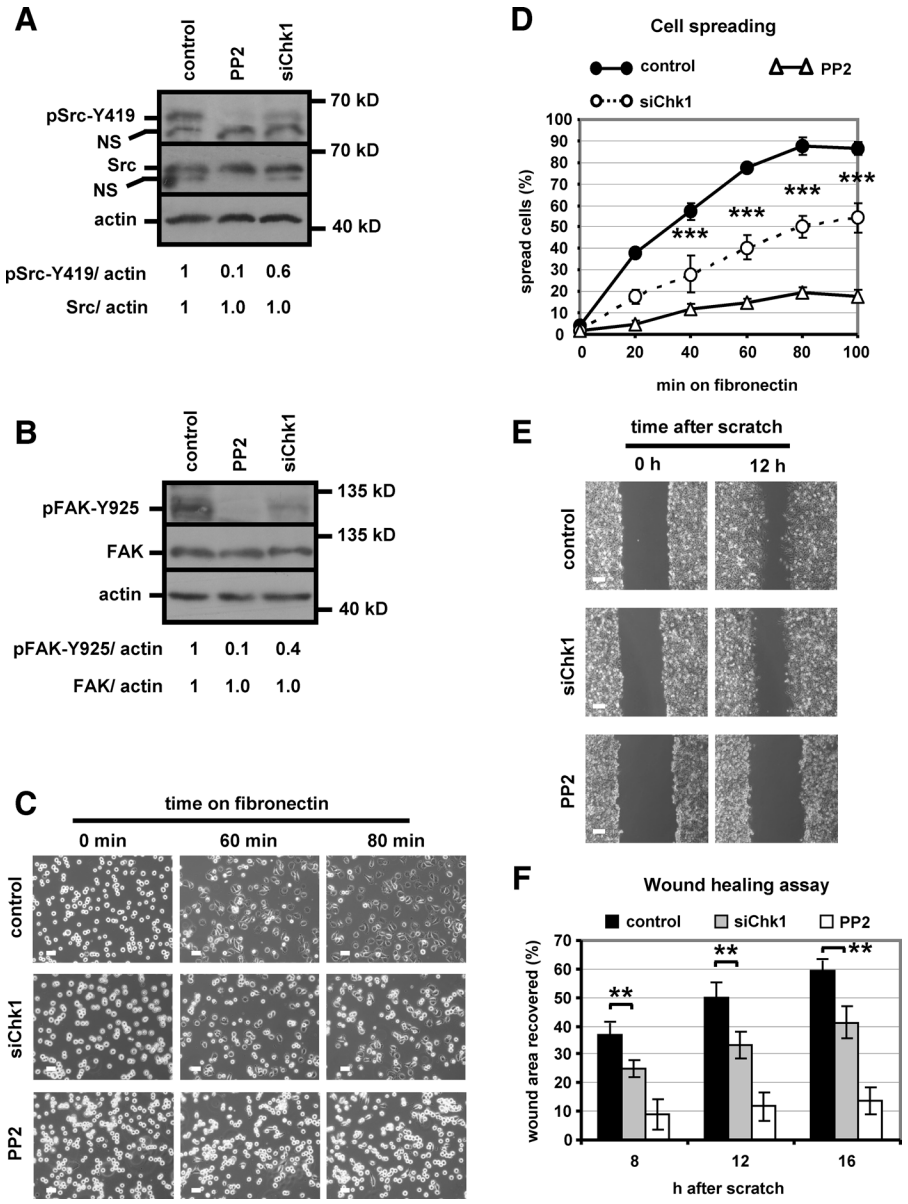

Figure 7. **Chk1-inhibition reduces Src kinase activity. (A and B)** Cells transfected with negative siRNA (control) or siChk1 were trypsinized and seeded on fibronectin-coated dishes in the absence or presence of PP2 for 1 h. Western blot analysis of total phospho–Src-Y419 (pSrc-Y419), Src, phospho–FAK-Y925 (pFAK-Y925), FAK, or actin. NS, nonspecific. Relative band intensity values are shown, and values in control were set to 1. **(C)** Chk1 depletion reduces cell spreading. Cells were seeded on fibronectin-coated dishes and phase-contrast images taken at various times after plating. Bars, 50 µm. **(D)** Percentage of spread cells (i.e., flattened and not highly reflective) from C. Error bars show the SD from the mean from three independent experiments. Approximately 750–1,000 cells were analyzed per experiment. **(E)** Cells were seeded on fibronectin-coated dishes and analyzed by wound healing assay. Phase-contrast images at 0 h and 12 h after wounding are shown. Bars, 200 µm. **(F)** Wound area covered calculated from cells as in E. Error bars show the SD from the mean from four independent experiments. **, $P < 0.01$; ***, $P < 0.001$ compared with the control. Statistically significant differences were determined by ANOVA and Student's *t* test.

Chk1 is required for Src-S51 phosphorylation in cultured cells

Confocal microscopy analysis showed that phosphorylated Src-S51 localized to actin patches in control cells with chromatin bridges (Figs. 9 B and S4 F). Depletion of Src by siRNA diminished phospho-S51 staining compared with control cells (Fig. 9 B). Furthermore, phospho-S51 staining was impaired after incubation of the anti–pSrc-S51 antiserum with the phosphorylated peptide phospho-S51 compared with the unphosphorylated peptide S51 synthetic peptides (Fig. S4 F), verifying that this reagent is specific for the phosphorylated Src-S51 in immunofluorescence. Phosphorylated Src-S51 also localized to membrane ruffles, filopodia, and the nucleus and partially colocalized with vinculin at focal adhesions in interphase cells on fibronectin, in the absence of chromatin bridges (Figs. 9 C and S5, A and B). Depletion of Chk1 diminished Src-S51 phosphorylation compared with control cells in the absence or presence of DNA bridges, showing that S51 phosphorylation is Chk1-dependent (Fig. 9, B–D). Chk1 was precipitated from cell extracts using an antibody against the endogenous Src and associated with GST-Src but not with GST in pulldown experiments (Figs. 9 E and S5 C). These results suggest that Chk1 associates with Src and phosphorylates Src-S51 in interphase cells.

Phosphorylated Src-S51 prevents chromatin breakage

In cells depleted of the endogenous Src by siSrc-2, expression of the phosphomimetic mutant S51D but not WT GFP-Src resistant to degradation by siSrc-2 prevented chromatin breakage and rescued formation of actin patches after Chk1 depletion compared with Chk1-proficient controls (Fig. 10, A and C). Furthermore, GFP–Src-S51D localized to actin patches in Chk1-deficient or control cells (Fig. 10 A). In contrast, expression of the nonphosphorylatable mutant Src–GFP-S51A induced chromatin breakage and diminished formation of actin patches in the absence or presence of siChk1 (Fig. 10, A–D). We propose that Chk1-mediated Src-S51 phosphorylation is required for actin patch formation and inhibition of chromatin breakage in late cytokinesis. Also, expression

Downloaded from http://rupress.org/jcb/article-pdf/217/9/3071/1614074/jcb_201802102.pdf by guest on 08 February 2026

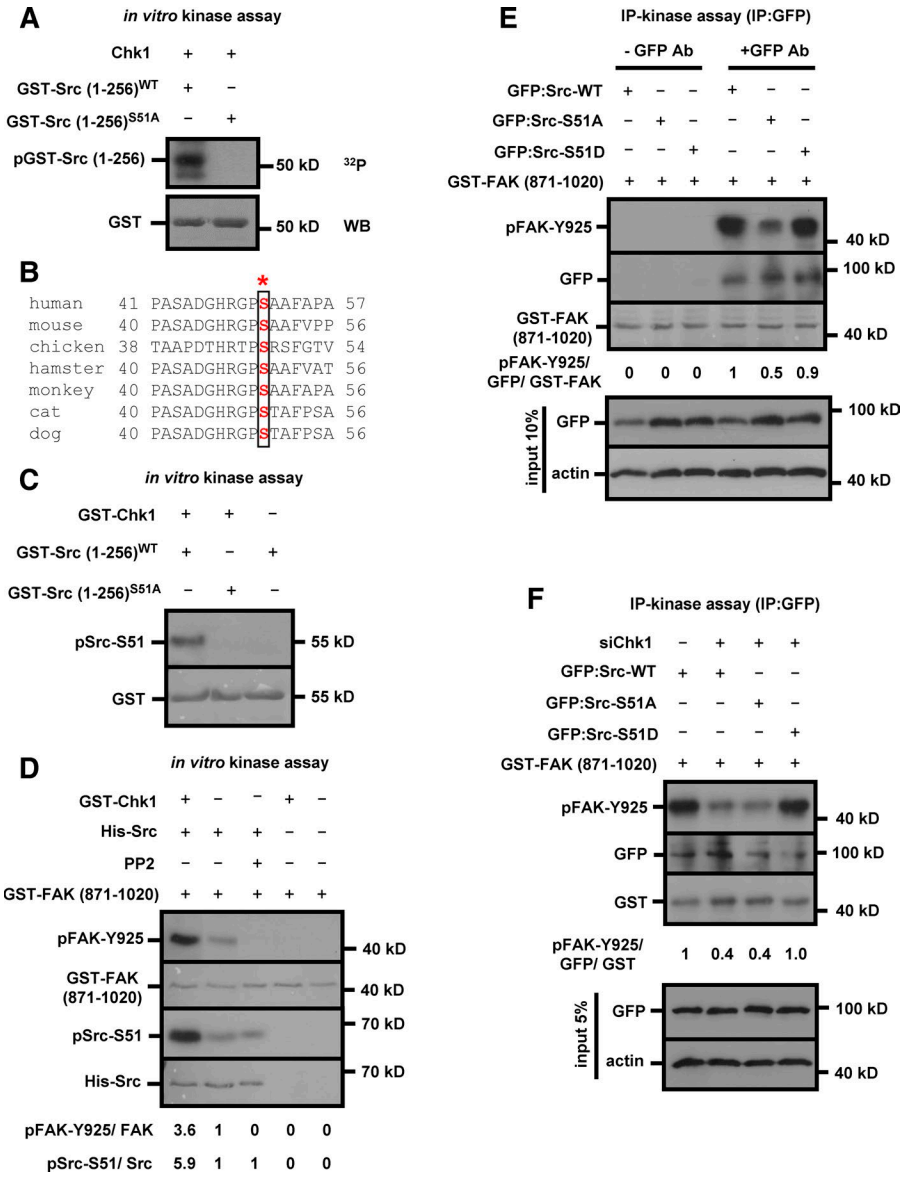

Figure 8. **Mutation of human Src-S51 to alanine reduces Src catalytic activity. (A)** Chk1 kinase assay. Top: Autoradiography analysis (^{32}P) of phosphorylated Src using purified WT or S51A GST-Src (1–256) substrate. Bottom: Western blot (WB) analysis of total GST. Top and bottom panels are from the same gel. **(B)** Alignment of Src protein sequences. Human serine 51 is marked by an asterisk. **(C)** Chk1 in vitro kinase assay. Western blot analysis of phosphorylated (pSrc-S51) by using the anti-pS51 antiserum along with total GST-Src. **(D)** In vitro kinase assay using recombinant GST-Chk1, His-Src, and purified GST-FAK (871–1020) as substrate. Western blot analysis of phosphorylated FAK-Y925 (pFAK-Y925) and pSrc-S51 using phosphospecific antibodies, and Ponceau staining of GST-FAK (871–1020) and His-Src. Relative band intensity values are shown, and values in the second lane from left (His-Src) were set to 1. **(E)** Immunoprecipitation (IP) kinase assay using GST-FAK (871–1020) as substrate. Top: Western blot analysis of GFP-associated FAK-Y925 phosphorylation and immunoprecipitated GFP, and Ponceau staining of GST-FAK (871–1020). Bottom: Western blot analysis of total GFP and actin. Relative band intensity values are shown, and values in GFP–Src-WT were set to 1. Ab, antibody. **(F)** Immunoprecipitation-kinase assay in the absence or presence of siChk1. Top: Western blot analysis of GFP-associated FAK-Y925 phosphorylation, immunoprecipitated GFP, and GST-FAK (871–1020). Bottom: Western blot analysis of total GFP and actin. Relative band intensity values are shown, and values in GFP–Src-WT without siChk1 were set to 1.

of S51D GFP-Src increased the number of filopodia in interphase cells without DNA bridges compared with cells expressing GFP only (Fig. S5, D and E), in agreement with previous studies showing that Src catalytic activity promotes filopodia formation (Robles et al., 2005; He et al., 2015).

Discussion

Control cells with chromatin bridges delay abscission and retain actin patches at the base of the chromatin bridge/intercellular canal; however, the molecular mechanisms of actin patch formation have not been previously reported (Chen and Doxsey, 2009; Steigemann et al., 2009). In this study, we show that Src, a nonreceptor tyrosine kinase that is involved in actin remodeling (Frame, 2002; Playford and Schaller, 2004), and Chk1, a kinase that functions in different stages of the cell cycle (Zhang and Hunter, 2014), prevent chromosome breakage and are required for formation of actin patches in cytokinesis. Chromatin breakage in Chk1- or Src-deficient cells is not caused by abscission as evidenced by the majority of cells exhibiting broken chromatin with an intact intercellular canal and also by the inability of a dominant-negative Vps4-K173Q protein that inhibits abscission to prevent chromatin bridges from breaking (Morita et al., 2007; Petsalaki and Zachos, 2016). Although a potential function for Chk1 and Src in DNA breakage that is independent of their role in regulating actin patches cannot be formally excluded, our results are consistent with Chk1 and Src preventing DNA bridges from breaking by promoting formation of actin patches. A minority of Chk1- or Src-deficient cells exhibit both fragmented chromatin bridges and broken intercellular canals; this could be caused by reduced stability of the intercellular canal in the absence of actin patches or by weakening of the abscission checkpoint after chromatin breakage, perhaps because of released membrane tension or the broken chromatin being reeled in from the canal (Lafaurie-Janvore et al., 2013; Nähse et al., 2017). In addition, Chk1 or Src inhibition exacerbates chromatin breakage in Aurora B–deficient cells with an impaired abscission checkpoint (Steigemann et al., 2009), and this correlates with reduced actin patches and with

Downloaded from http://rupress.org/jcb/article-pdf/217/9/3071/1614074/jcb_201802102.pdf by guest on 08 February 2026

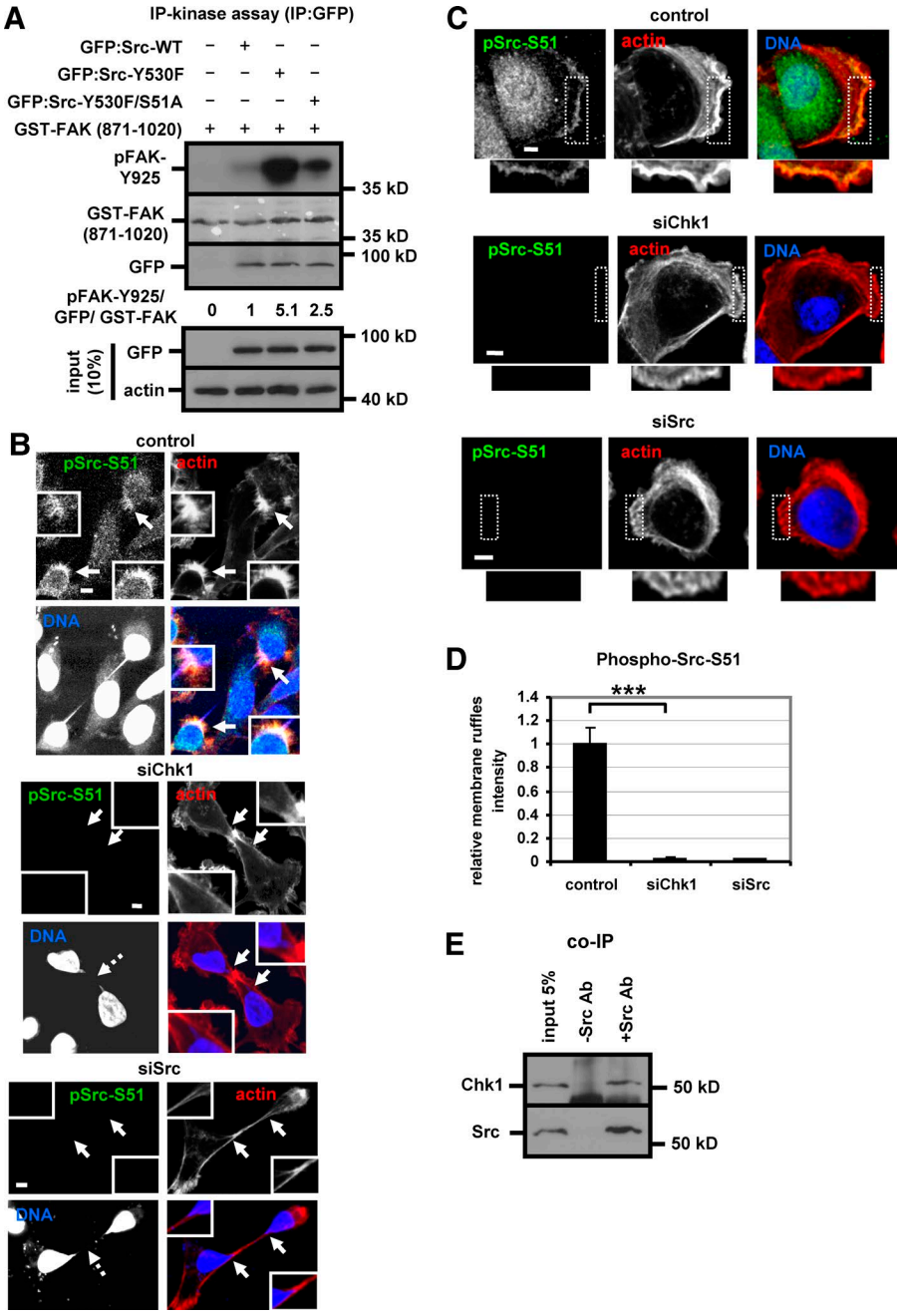

Figure 9. **Chk1 depletion reduces Src-S51 phosphorylation. (A)** Immunoprecipitation (IP) kinase assay using GST-FAK (871–1020) as substrate. Top: Western blot analysis of GFP-associated FAK-Y925 phosphorylation (pFAK-Y925) and immunoprecipitated GFP as well as Ponceau staining of GST-FAK (871–1020). Bottom: Western blot analysis of total GFP and actin. Relative band intensity values are shown, and values in GFP–Src-WT were set to 1. **(B)** Localization of phosphorylated Src-S51 (pSrc-S51). Cells were transfected with negative siRNA (control), siChk1, or siSrc. Broken DNA bridges are indicated by dotted arrows, and the bases of the intercellular canals are indicated by solid arrows. Insets show 1.6× magnification of the canals bases. Images are representative of 20 cells from two independent experiments. **(C)** Cells transfected as in B were seeded on fibronectin-coated slides for 1 h. Insets show 2× magnification of membrane ruffles. Bars, 5 µm. **(D)** Phosphorylated Src-S51 at membrane ruffles. Relative green fluorescence intensity from C is shown, and values in control were set to 1. Error bars show the SD from the mean. $n = 20$ cells from two independent experiments. ***, $P < 0.001$ compared with the control. Statistically significant differences were determined by ANOVA and Student's t test. **(E)** Coimmunoprecipitation from asynchronous cells. Chk1 or Src were detected by Western blotting. Ab, antibody.

increased frequency of double-deficient cells exhibiting chromosome breakage in the presence of an intact midbody compared with cells depleted of Aurora B only. We propose that actin patch formation by Chk1 and Src cooperates with the Aurora B–imposed abscission delay to prevent chromatin breakage. These results also suggest that Chk1 and Src are not essential for the abscission delay in response to chromatin bridges. Because Chk1 is required for abscission delay after replication stress, one possibility is that replication stress and chromatin trapped at the intercellular canal can trigger separate signaling pathways that can converge on Aurora B to impose the abscission checkpoint (Mackay and Ullman, 2015; Nähse et al., 2017).

We also show that Chk1 is required for optimal localization and complete activation of Src, efficient cell spreading, and wound healing on fibronectin. Chk1 associates with Src and phosphorylates human Src at the conserved serine 51 inside the Src-Unique region. Phosphorylated Src-S51 localizes to membrane ruffles, filopodia, and the nucleus. Also, phosphorylated Src-S51 and Src-signaling proteins such as phosphorylated FAK-Y925 and cortactin localize to actin patches in control cells with chromatin bridges. Mutation of S51 to a nonphosphorylatable alanine residue reduces Src catalytic activity by ∼50% compared with the WT protein, diminishes actin patches, and induces chromatin breakage. In addition, expression of a phosphomimetic Src-S51D protein rescues formation of actin patches and prevents chromatin breakage in Chk1-deficient cells.

On the basis of these findings, we propose the following model (Fig. 10 E): Chk1 phosphorylates Src at serine 51, and

Downloaded from http://rupress.org/jcb/article-pdf/217/9/3071/1614074/jcb_201802102.pdf by guest on 08 February 2026

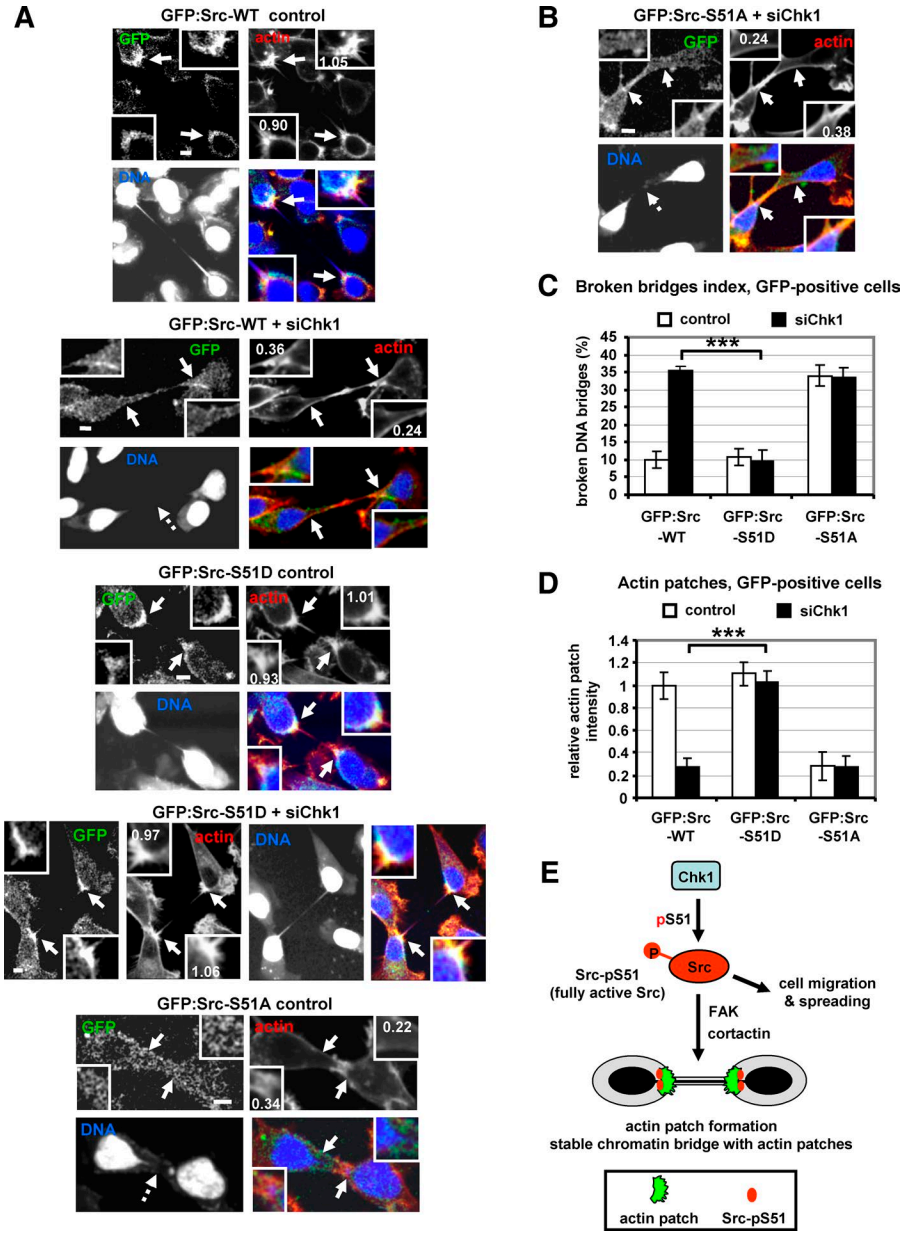

Figure 10. **Expression of the phosphomimetic Src-S51D mutant rescues formation of actin patches and prevents chromatin breakage in Chk1-deficient cells. (A and B)** Cells expressing WT, S51D, or S51A GFP-Src resistant to degradation by siSrc-2 were depleted of the endogenous Src by siSrc-2 and transfected with negative siRNA (control) or siChk1. Broken DNA bridges are indicated by dotted arrows, and the bases of the intercellular canals are indicated by solid arrows. Relative actin patch intensity values are shown. Insets show 1.6× magnification of the canals bases. Bars, 5 µm. **(C)** Percentage of DNA bridges that appear broken in GFP-positive cells. Error bars show the SD from the mean from three independent experiments. A minimum of 30 cells with chromatin bridges was analyzed per experiment. **(D)** Actin patches intensity. Relative red fluorescence from A and B is shown, and values in GFP–Src-WT control were set to 1. Error bars show the SD from the mean. n = 30 cells from three independent experiments. ***, $P < 0.001$ compared with the control. Statistically significant differences were determined by ANOVA and Student's t test. **(E)** Model for the role of Chk1 and Src in cytokinesis with chromatin bridges. p, phosphorylation.

this phosphorylation is required for optimal Src localization, complete Src kinase activity, and efficient cell migration and spreading. Furthermore, in the presence of chromatin bridges, phosphorylated Src-S51 and Src-signaling proteins promote formation of actin patches and prevent chromosome breakage in cytokinesis.

Phosphorylation of serine 51 can promote Src kinase activity independently of Src-Y530 phosphorylation. Structurally, the Y530F mutant of Src remains 85% in its inactive closed form, and the SH3 domain of Src can down-regulate Src kinase activity in the absence of Y530 phosphorylation through interactions with the kinase N-terminal lobe (Xu et al., 1999; Brábek et al., 2002; Bernadó et al., 2008). The Src-SH3 domain also interacts with the Unique domain through a binding region in the opposite side of the SH3 peptide binding site, and the SH3–Unique domain interaction is lost after addition of a high-affinity SH3 ligand peptide that induces the active open conformation of the kinase (Maffei et al., 2015). Therefore, one possibility is that S51 phosphorylation activates Src by destabilizing the interaction between the SH3 and the Unique domain to promote the open conformation. In addition, because S51 is inside the unique domain lipid binding region, S51 phosphorylation may modulate interactions between the Unique domain and lipids to regulate Src localization (Pérez et al., 2013; Amata et al., 2014).

How do actin patches stabilize chromatin bridges? The oval or heart shape of many of the nuclei in telophase cells with chromatin bridges suggests that considerable pulling forces are exerted by the chromosomes in the bridge. These forces could cause chromatin breakage by mechanical rupture or induce transient nuclear envelope rupture during interphase, followed by bridge resolution by nuclease activity (Ganem and Pellman, 2012; Maciejowski et al., 2015). Perhaps, intriguingly, breakage of chromatin bridges in cells proficient for the abscission checkpoint preferentially occurs next to centromeres at the foot of the

Downloaded from http://rupress.org/jcb/article-pdf/217/9/3071/1614074/jcb_201802102.pdf by guest on 08 February 2026

DNA bridge, around where actin patches are formed, indicating this chromatin region is under relatively high tension (Hoffelder et al., 2004; Petsalaki et al., 2014; Lopez et al., 2015). One possibility is that the dense meshwork of highly organized actin filaments inside the actin patches provides mechanical support to the nuclear envelope and underlying chromatin by increasing the stiffness and elasticity at the base of the chromatin bridge to counteract the pulling forces applied by the chromosomes in the bridge. Because cross-linkers affect the architecture and mechanical properties of the actin network, identifying how actin filaments are organized and linked together inside the patches may help us understand how such forces are acting (Fletcher and Mullins, 2010).

Phosphorylated FAK-Y925 and cortactin were also detected at actin patches. Focal adhesion proteins are involved in mechanotransduction and can promote force-dependent actin polymerization (Geiger et al., 2009; Houk et al., 2012). Investigating which Src-signaling proteins are required for actin patch formation in response to DNA bridges may help us better understand how cells stabilize chromatin bridges. In conclusion, our study identifies novel proteins that promote formation of actin patches and protect against chromatin breakage in cytokinesis.

Materials and methods

Antibodies

Anti-pS51 polyclonal antiserum was generated in rabbits by immunization against the phosphorylated peptide phospho-S51 (DGHRGP[pSER]AAFAPAAC) of human Src (Genscript). The unphosphorylated peptide S51 (DGHRGPSAAFAPAAC) was used in competition experiments as appropriate.

Mouse monoclonal antibodies against GST (B-14), Chk1 (G-4), FAK (D-1), cortactin (H-5), vinculin (7F9), and Cep55 (B-8; sc-374051) were from Santa Cruz Biotechnology. Rabbit polyclonal antibodies against GFP (full length; sc-8334), c-Src (N-16; sc-19 used in immunofluorescence), Plk1 (H-152; sc-5585), and Mklp1 (N-19; sc-867) were also from Santa Cruz Biotechnology. Rabbit polyclonal antibodies against Aurora B (ab2254) and Src (ab109381, used in Western blotting) were from Abcam, rabbit polyclonal antibody against phospho–Src-Y419 (Src [pY418], 44660G) was from Invitrogen, and mouse monoclonal antiphospho–histone H2A.X (S139; clone JBW301; γ-H2AX) was from EMD Millipore (05-636). Mouse monoclonal antibodies against α-tubulin (DM1A) and actin (AC-40) were from Sigma-Aldrich, mouse monoclonal anti–lamin B2 (E-3) was from Thermo Fisher Scientific (33-2100), and rabbit polyclonal antibody against phospho–FAK-Y925 (AF44671) was from R&D Systems.

Plasmids and cloning

Plasmid pEGFP/c-Src encoding WT human c-Src (1–536 with 1 designating the initiator methionine) fused to EGFP into pcDNA4/TO vector (Invitrogen) was a gift from N. Yamagushi (Chiba University, Chiba, Japan; Kasahara et al., 2007b). Plasmid pEGFP/av c-Src encoding the full length chicken c-Src fused to EGFP into pEGFP-N1 vector (Takara Bio Inc.) was from M. Resh (Memorial Sloan-Kettering Cancer Center, New York, NY; Donepudi and Resh, 2008), and plasmid pEGFP/FAK encoding full-length human FAK N-terminally fused to GFP into pCS105 (Addgene) was from P. Skourides (University of Cyprus, Nicosia, Cyprus). Plasmid pEGFP-vps4-K173Q encoding human VPS4 harboring the K173Q point mutation fused to EGFP into pEGFP-C1 vector (Takara Bio Inc.) was a gift from W. Sundquist (University of Utah, Salt Lake City, UT; Morita et al., 2007), and plasmid pEGFP-N1 coding for GFP under cytomegalovirus promoter was obtained from Takara Bio Inc.

Plasmid pEGFP/Chk1 encoding human Chk1 fused to EGFP into pEGFP-N1 vector (Takara Bio Inc.) was from Addgene (22888; Unsal-Kaçmaz et al., 2005). Sequencing of this plasmid showed that Chk1 exhibited mutation of aspartic acid-130 to alanine (D130A), and this mutation was reversed to obtain the WT pEGFP/Chk1 plasmid.

To generate the pGEX4T1/av c-Src vector encoding GST-tagged avSrc, a full-length avian c-Src cDNA sequence was amplified by PCR by using pEGFP/av c-Src as template and cloned into the pGEX4T1 vector (GE Healthcare) as a BamHI-EcoRI fragment. To generate pGEX4T1/c-Src or pGEX4T1/c-Src (1–256) vectors encoding GST-tagged full-length or truncated human Src, a human c-Src cDNA sequence was amplified by PCR using pEGFP/c-Src as template and cloned into the pGEX4T1 vector with EcoRI-XhoI. To generate pGEX4T1/FAK (871–1020) encoding a GST-tagged truncated form of human FAK, FAK cDNA sequence was amplified by PCR using pEGFP/FAK as a template and cloned into the pGEX4T1 vector with BamHI-XhoI. All plasmids were completely sequenced.

siRNA sequences

Negative siRNAs (a pool of four different siRNAs: 5′-UAAGGCUAUGAAGAGAUAC-3′, 5′-AUGUAUUGGCCUGUAUUAG-3′, 5′-AUGAACGUGAAUUGCUCAA-3′, and 5′-UGGUUUACAUGUCGACUAA-3′) were from Thermo Fisher Scientific/GE Healthcare. Human Chk1 (a pool of four different siRNAs: 5′-CAAGAUGUGUGGUACUUUA-3′, 5′-GAGAAGGCAAUAUCCAAUA-3′, 5′-CCACAUGUCCUGAUCAUAU-3′, and 5′-GAAGUUGGGCUAUCAAUGG-3′), Chk1-2 (5′-CCACAUGUCCUGAUCAUAU-3′), Src-2 (5′-GCAGUUGUAUGCUGUGGUU-3′), and Aurora B (5′-CCAAACUGCUCAGGCAUAA-3′) siRNAs were also from Thermo Fisher Scientific/GE Healthcare. Human Src (a pool of four different siRNAs: 5′-CUCGGCUCAUUGAAGACAA-3′, 5′-UGACUGAGCUCACCACAAA-3′, 5′-CCUCAUCAUAGCAAUAACA-3′, and 5′-GUAGAUUUCAGAUGACUAU-3′) siRNAs were obtained from Santa Cruz Biotechnology. Only the sense sequences of the siRNA duplexes are shown.

Mutagenesis

Point mutations were generated by using the Q5 site-directed mutagenesis kit (New England Biolabs). To generate siRNA-resistant forms of GFP-Src, the pEGFP/c-Src coding for human GFP-Src was used to introduce T982C, G984A, and T987C point mutations giving resistance to the Src-2 siRNA. This plasmid was then used to make A151G and G152C point mutations changing Src-S51 to alanine or A151G and G152A point mutations changing Src-S51 to aspartic acid. For changing Src-Y530 to phenylalanine, the pEGFP/c-Src plasmid was used to make the A1589T point mutation. To revert the D130A mutation on human GFP-Chk1, the pEGFP/Chk1 plasmid from Addgene (22888) was used to make a

Downloaded from http://rupress.org/jcb/article-pdf/217/9/3071/1614074/jcb_201802102.pdf by guest on 08 February 2026

C389A point mutation changing the Chk1-A130 to aspartic acid and generate the WT GFP-Chk1 protein. To generate siRNA-resistant forms of GFP-Chk1, the WT pEGFP/Chk1 plasmid was used to introduce A1044C, T1047C, and T1050A point mutations giving resistance to the Chk1-2 siRNA.

Recombinant and purified proteins

Recombinant human GST-Chk1 (14-346) and His-Src (14-326) were from EMD Millipore. GST-tagged proteins were expressed in BL21 (DE3) cells (Agilent Technologies) and purified by using glutathione-agarose beads (Santa Cruz Biotechnology) or were eluted from beads by using the GST spintrap purification module (GE Healthcare).

Cell culture and treatments

Human colon carcinoma BE cells (a gift from S. Wilkinson and C. Marshall, Institute of Cancer Research, London, UK; Petsalaki et al., 2018) and cervical carcinoma HeLa cells stably expressing LAP2b fused to RFP (a gift from D. Gerlich, Institute of Molecular Biotechnology, Vienna, Austria; Steigemann et al., 2009) were grown in DMEM (Gibco) containing 10% FBS at 37°C in 5% CO_2. Cells were treated with 300 nM UCN-01 (U6508; Sigma-Aldrich), 10 µM PP2 (1407; Tocris Bioscience), or 1 µM TG003 (T5575; Sigma-Aldrich) as appropriate. Negative siRNA or siRNA duplexes designed to repress human Chk1, Src, or Aurora B were transfected into BE cells 24 h before analysis using Lipofectamine 2000 (Invitrogen). For expression of GFP proteins, plasmids were transfected into cells in the absence or presence of appropriate siRNA duplexes 24 h before analysis or further drug treatment using Turbofect (Thermo Fisher Scientific). All cell lines used exhibited consistent morphology and growth properties and were negative for mycoplasma contamination.

Coating with fibronectin

Petri dishes or slides were incubated with 1 µg/ml fibronectin (EMD Millipore) for 1 h at 37°C before use.

Time-lapse imaging

BE or HeLa LAP2b-RFP cells were seeded onto Petri dishes with a 30-mm glass base (Greiner), and an inverted fluorescence microscope (Observer D1; Zeiss) was used. Fluorescence and phase-contrast images were taken by using a 63× Plan Neofluor 0.75 NA Ph2 dry objective (Zeiss; Figs. 1 E and S1 C), a 20× Plan Neofluor 0.40 NA Ph2 dry objective (Zeiss; Fig. 7, C and D), or a 10× A-plan 0.25 Ph1 dry objective (Zeiss; Fig. 7, E and F). Imaging was performed at 37°C in 5% CO_2 by using a Zeiss AxioCam MRm camera and the Zeiss ZEN 2 acquisition software. For UCN-01 or PP2 treatments in Figs. 1 and 7, the drugs were added to the medium immediately before filming.

Cell spreading assay

Confluent cells were trypsinized and counted, and 1 × 10^6 BE cells were plated on fibronectin-coated 35-mm dishes. Cells were photographed every 20 min at 37°C in 5% CO_2 by using a Zeiss AxioCam MRm camera (see the Time-lapse imaging section), and the percentage of spread cells (i.e., cells that were flattened and relatively less reflective) was calculated at various times. The method was adapted from Brunton et al. (2005).

Wound healing assay

Fibronectin-coated 35-mm dishes containing a confluent monolayer of cells were used, and a wound was created by scraping the monolayer with a yellow gel loading tip. The dish was subsequently washed with warm PBS and the wound area photographed at desired time points (0–16 h) at 37°C in 5% CO_2 by using an AxioCam MRm camera. The wound area without cells was measured using a region/polygon tool (ZEN 2 software), and the percentage of wound area recovered (wound closure) was calculated. The method was adapted from Elias et al. (2010).

Indirect immunofluorescence microscopy

For intercellular canal labeling with FM 1-43FX, see Intercellular canal labeling. For all other fluorescence microscopy applications, cells were fixed in 4% paraformaldehyde in cytoskeleton buffer (1.1 M Na_2HPO_4, 0.4 M KH_2PO_4, 137 mM NaCl, 5 mM KCl, 2 mM $MgCl_2$, 2 mM EGTA, 5 mM Pipes, and 5 mM glucose, pH 6.1) for 5 min at 37°C, permeabilized in 0.5% Triton X-100 in cytoskeleton buffer, washed twice with PBS at room temperature, and immunostained. For peptide competitions, 2.2 µg of the anti-pS51 polyclonal antiserum was incubated with 100 µg peptide at 37°C for 1 h, and then used for immunostaining.

FITC- or rhodamine-TRI TC-conjugated secondary antibodies (Jackson ImmunoResearch Laboratories, Inc.) were used as appropriate. DNA was stained with 10 µM TO-PRO-3 iodide (642/661 nm; Invitrogen), and cells were mounted in Vectashield medium (Vector Laboratories). Images were collected by using a laser-scanning spectral confocal microscope (TCS SP2; Leica Microsystems), LCS Lite software (Leica Microsystems), and a 63× Apochromat 1.40 NA oil objective. The low-fluorescence immersion oil (11513859; Leica) was used, and imaging was performed at room temperature. Mean projections of image stacks were obtained by using the LCS Lite software.

Intercellular canal labeling

Cells were incubated with 5 µg/ml FM 1-43FX fluorescence dye (F35355; Thermo Fisher Scientific/Invitrogen) in ice-cold Opti-MEM medium (11058021; Thermo Fisher Scientific) for 5 min at 4°C. The dye was then removed, and the cells were fixed with ice-cold 4% paraformaldehyde in cytoskeleton buffer for 10 min at 4°C. Next, the cells were permeabilized with 0.5% Triton X-100 in warm (37°C) cytoskeleton buffer for 5 min at room temperature, washed three times with warm (37°C) PBS, and stained with 10 µM TO-PRO-3 iodide (Invitrogen).

Quantification of fluorescence signals

Fluorescence intensity signals at midbodies were quantified using the LCS Lite ellipse tool by analyzing an image area of 2 μm^2 around each midbody, and intensity values were normalized versus values obtained by analyzing an identical area within the cell immediately adjacent on the midbody (Waters, 2009; Petsalaki and Zachos, 2016).

Actin patch-fluorescence intensity signals were quantified using the LCS Lite polygon tool by analyzing an image area of

Downloaded from http://rupress.org/jcb/article-pdf/217/9/3071/1614074/jcb_201802102.pdf by guest on 08 February 2026

40 µm² around the base of the DNA bridge, and intensity values were normalized versus values obtained by analyzing an identical area within the cell near the base of the DNA bridge (Waters, 2009).

DNA bridge-fluorescence intensity signals were quantified using the LCS Lite polygon tool by analyzing an image area encompassing the entire DNA bridge or intercellular canal, and intensity values were normalized versus values obtained by analyzing an identical area outside the canal. For weak versus strong DNA staining, DNA bridge-fluorescence intensity signals from 40 control bridges were quantified, and the mean value was set to 0.5. DNA bridges exhibiting relative fluorescence intensity >0.5 were taken as strong, whereas those exhibiting relative fluorescence intensity <0.5 were classified weak DNA signals.

Fluorescence intensity signals at membrane ruffles were quantified using the LCS Lite polygon tool by analyzing an image area of 100 µm² around the membrane, and intensity values were normalized versus values obtained by analyzing an identical area within the cell immediately adjacent on the membrane (Waters, 2009).

Mass spectrometry

GST–avSrc bands were excised from the gel and digested with trypsin, and the extracted tryptic peptides were analyzed by liquid chromatography–mass spectrometry as described previously (Ducommun et al., 2015). The data were searched against an in-house database containing the avian c-Src sequence using Mascot (2.4.1; Matrix Science) and MaxQuant (1.3.8.2). All result files were loaded into Scaffold (4.8.4; Proteome Software Inc.). Protein thresholds were set to 95.0% with a two unique peptide threshold to report protein identification. Peptide identifications were accepted if they could be established at >95.0% probability as specified by the Peptide Prophet algorithm (Keller et al., 2002), resulting in a peptide false discovery rate of 0.76%.

In vitro kinase assays

For the in vitro Chk1 kinase assays in Figs. 8 A and S4 A, 0.5 µg recombinant GST-Chk1 was incubated with 1 µg GST-Src protein substrate in 20 µl Chk1 kinase buffer (20 mM MOPS, pH 7.2, 5 mM EGTA, 10 mM $MgCl_2$, 25 mM sodium β-glycerophosphate, 1 mM sodium vanadate, 1 mM DTT, 100 µM ATP, and 1 µCi γ-^{32}P ATP) for 20 min at 30°C before analysis by SDS-PAGE. Radioactive labeling of Chk1 substrates was determined by autoradiography. The in vitro Chk1 kinase assay in Fig. 8 C was as above except that the γ-^{32}P ATP was omitted from the reaction mixture, and phosphorylation of Chk1 substrates was determined by Western blotting using an antiserum against phospho–Src-S51.

For the in vitro kinase assays in Figs. 8 D and S4 (C and D), 0.5 µg recombinant GST-Chk1 and 0.5 µg recombinant His-Src were incubated with 1 µg GST-FAK (871-1020) protein substrate eluted from beads in 20 µl Src kinase buffer (40 mM MOPS, 1 mM EDTA, and 0.1 mM ATP) for 30 min at 30°C before analysis by SDS-PAGE. Labeling of the GST-FAK (871–1020) substrate was determined by Western blotting using an antibody against phospho–FAK-Y925, and Src-S51 phosphorylation was determined by Western blotting using an antiserum against phospho–Src-S51. Where appropriate, 145 ng UCN-01 or 3 µg PP2 were included in the kinase reaction.

GFP immunoprecipitation and kinase assay

For GFP immunoprecipitations (Fig. 8, E and F), cells were sonicated three times for 10 s in ice-cold immunoprecipitation/kinase buffer (50 mM Hepes, pH 7.5, 150 mM NaCl, 1 mM EDTA, 2.5 mM EGTA, 10% glycerol, 0.1% Tween 20, 0.1 mM PMSF, 10 µg/ml leupeptin, 10 µg/ml aprotinin, 1 mM sodium fluoride, 10 mM sodium β-glycerophosphate, and 0.1 mM sodium vanadate) and incubated for another 30 min on ice. 1 mg cell lysate was incubated with 0.5 µg anti-GFP antibody for 16 h followed by the addition of 10 µl protein A/G PLUS–agarose beads (Santa Cruz Biotechnology) for 1 h at 4°C. Samples were spun down and washed three times with immunoprecipitation/kinase buffer and three times with Src reaction buffer (40 mM MOPS and 1 mM EDTA). Immunoprecipitated proteins on agarose beads were included in a 20-µl reaction in Src reaction buffer containing 1 µg GST-FAK (871–1020) eluted from beads and 0.1 mM ATP for 30 min at 30°C before analysis by SDS-PAGE. Labeling of the GST-FAK (871–1020) substrate was determined by Western blotting using an antibody against phospho–FAK-Y925.

Protein coimmunoprecipitations and GST-pulldown assays

Cells were lysed as described in the previous section. For coimmunoprecipitations, 1 mg cell lysate was incubated with 1 µg antibody for 16 h followed by the addition of 10 µl protein A/G PLUS–agarose beads for 1 h at 4°C. For GST pulldowns, 1 mg cell lysate was incubated with 1 µg GST-protein on glutathione-agarose beads for 4 h at 4°C. Samples were spun down and washed three times with immunoprecipitation/kinase buffer, and immunoprecipitated proteins on agarose beads were analyzed by SDS-PAGE and Western blotting.

Western blotting

Cells were lysed in ice-cold, whole-cell extract buffer (20 mM Hepes, 5 mM EDTA, 10 mM EGTA, 0.4 M KCl, 0.4% Triton X-100, 10% glycerol, 5 mM NaF, 1 mM DTT, 5 µg/ml leupeptin, 50 µg/ml PMSF, 1 mM benzamidine, 5 µg/ml aprotinin, and 1 mM Na_3VO_4) for 30 min on ice. Lysates were cleared by centrifugation at 15,000 *g* for 10 min, analyzed by SDS-PAGE, and transferred onto nitrocellulose membrane (Santa Cruz Biotechnology).

Densitometry

Densitometric analysis of bands was performed using ImageJ (National Institutes of Health).

Statistical analysis

For broken DNA bridges indices, 50 cells per experiment from three independent experiments were scored blindly, and the SD was calculated ($n = 150$). For broken DNA bridges indices in cells transfected with GFP-proteins, 30 GFP-positive cells per experiment from three independent experiments were scored blindly, and the SD was calculated ($n = 90$). For actin patches fluorescence in Figs. 2 E, 3 F, 5 C, and 10 D, 30 cells from three independent experiments were examined ($n = 30$), and the SD was calculated. For actin patches fluorescence in Figs. 3 B and S1 G, 20 cells from three or two independent experiments, respectively, were examined ($n = 20$), and the SD was calculated. For intact intercellular canals indices in Fig. 4 B, 15 cells with broken DNA bridges per

Downloaded from http://rupress.org/jcb/article-pdf/217/9/3071/1614074/jcb_201802102.pdf by guest on 08 February 2026

experiment from three independent experiments were examined ($n = 45$), and the SD was calculated. For intact midbodies indices in Fig. 5 D, at least 20 cells per experiment from three independent experiments were examined ($n > 60$), and the SD was calculated. For Plk1-, Cep55-, and Mklp1-associated fluorescence, 10 cells per experiment from two independent experiments were examined ($n = 20$), and the SD was calculated. For γ-H2AX micronuclei, a minimum of 150 cells per experiment from three independent experiments were examined ($n > 450$), and the SD was calculated. For cell spreading assays, ∼750–1,000 cells from five randomly chosen fields per experiment from three independent experiments were examined, and the SD was calculated ($n > 2{,}100$). For wound healing, one field per experiment from four independent experiments was examined ($n = 4$), and the SD was calculated. For phosphorylated Src-Y419, FAK-Y925, and Src-S51 fluorescence, cell membrane areas from 20 cells from two independent experiments ($n = 20$) were analyzed per treatment, and the SD was calculated. For filopodia formation (Fig. S5 E), the number of filopodia per cell from 15 cells from two independent experiments ($n = 15$) was determined, and the SD was calculated. Statistically significant differences between three or more groups were determined by one-way ANOVA followed by Student's *t* test between two groups. No statistical method was used to predetermine the sample size.

Online supplemental material

Fig. S1 shows the fluorescence intensity of actin patches in control, Chk1-deficient, or Src-deficient cells with intact DNA bridges. Fig. S1 also shows an example of control cells with a broken chromatin bridge, and Src-depleted cells with relatively strong or weak DNA bridge staining. Fig. S2 shows localization of Mklp1 and Cep55 to the midbody in control, Chk1-deficient, or Src-deficient cells in telophase or late cytokinesis. Fig. S3 shows localization of phosphorylated Src-Y419, phosphorylated FAK-Y925, and total Src at membrane ruffles in control, Chk1-deficient, or Src-deficient cells. Fig. S4 shows phosphorylation of avian GST-Src by recombinant Chk1 at newly identified sites in vitro. Fig. S4 also shows phosphorylations of Src-S51 and Src-Y419 in vitro in the presence of purified Chk1 and Src proteins, and specificity of the antiphospho-S51 antiserum in immunofluorescence. Fig. S5 shows localization of phosphorylated Src-S51 at focal adhesions and filopodia in interphase cells without chromatin bridges. Fig. S5 also shows Chk1 interaction with Src in GST pulldown experiments from cell extracts, and the number of filopodia per cell in cells expressing S51D GFP-Src. Video 1 shows a control HeLa LAP2b-RFP cell exhibiting a stable LAP2b intercellular bridge in cytokinesis. Video 2 shows a HeLa LAP2b-RFP cell exhibiting breakage of the LAP2b intercellular bridge in the presence of the Src family inhibitor PP2. Video 3 shows a HeLa LAP2b-RFP cell exhibiting breakage of the LAP2b intercellular bridge in the presence of the selective Chk1 inhibitor UCN-01.

Acknowledgments

We thank D. Gerlich, M. Resh, P. Skourides, W. Sundquist, and N. Yamagushi for sharing reagents.

This work was supported by Worldwide Cancer Research (grant 15-0008) and by Fondation Santé (review cycle 2017–2018). E. Petsalaki was supported by a postdoctoral fellowship from the Bodossaki Foundation, and M. Dandoulaki was supported by Worldwide Cancer Research. We also thank the Special Account for Research Funds of the University of Crete for paying the publication costs.

The authors declare no competing financial interests.

Author contributions: E. Petsalaki, M. Dandoulaki, and G. Zachos performed experiments and analyzed the results. D. Sumpton and S. Zanivan performed the mass spectrometry analysis. G. Zachos designed the study and wrote the paper.

Submitted: 17 February 2018
Revised: 16 April 2018
Accepted: 3 June 2018

References

Amata, I., M. Maffei, and M. Pons. 2014. Phosphorylation of unique domains of Src family kinases. *Front. Genet.* 5:181. https://doi.org/10.3389/fgene.2014.00181

Bastos, R.N., and F.A. Barr. 2010. Plk1 negatively regulates Cep55 recruitment to the midbody to ensure orderly abscission. *J. Cell Biol.* 191:751–760. https://doi.org/10.1083/jcb.201008108

Bernadó, P., Y. Pérez, D.I. Svergun, and M. Pons. 2008. Structural characterization of the active and inactive states of Src kinase in solution by small-angle X-ray scattering. *J. Mol. Biol.* 376:492–505. https://doi.org/10.1016/j.jmb.2007.11.066

Brábek, J., D. Mojzita, M. Novotný, F. Půta, and P. Folk. 2002. The SH3 domain of Src can downregulate its kinase activity in the absence of the SH2 domain-pY527 interaction. *Biochem. Biophys. Res. Commun.* 296:664–670. https://doi.org/10.1016/S0006-291X(02)00884-7

Brown, M.C., L.A. Cary, J.S. Jamieson, J.A. Cooper, and C.E. Turner. 2005. Src and FAK kinases cooperate to phosphorylate paxillin kinase linker, stimulate its focal adhesion localization, and regulate cell spreading and protrusiveness. *Mol. Biol. Cell.* 16:4316–4328. https://doi.org/10.1091/mbc.e05-02-0131

Brunton, V.G., E. Avizienyte, V.J. Fincham, B. Serrels, C.A. Metcalf III, T.K. Sawyer, and M.C. Frame. 2005. Identification of Src-specific phosphorylation site on focal adhesion kinase: dissection of the role of Src SH2 and catalytic functions and their consequences for tumor cell behavior. *Cancer Res.* 65:1335–1342. https://doi.org/10.1158/0008-5472.CAN-04-1949

Caballe, A., D.M. Wenzel, M. Agromayor, S.L. Alam, J.J. Skalicky, M. Kloc, J.G. Carlton, L. Labrador, W.I. Sundquist, and J. Martin-Serrano. 2015. ULK3 regulates cytokinetic abscission by phosphorylating ESCRT-III proteins. *eLife.* 4:e06547. https://doi.org/10.7554/eLife.06547

Capalbo, L., E. Montembault, T. Takeda, Z.I. Bassi, D.M. Glover, and P.P. D'Avino. 2012. The chromosomal passenger complex controls the function of endosomal sorting complex required for transport-III Snf7 proteins during cytokinesis. *Open Biol.* 2:120070. https://doi.org/10.1098/rsob.120070

Carlton, J.G., A. Caballe, M. Agromayor, M. Kloc, and J. Martin-Serrano. 2012. ESCRT-III governs the Aurora B-mediated abscission checkpoint through CHMP4C. *Science.* 336:220–225. https://doi.org/10.1126/science.1217180

Chen, C.T., and S. Doxsey. 2009. A last-minute rescue of trapped chromatin. *Cell.* 136:397–399. https://doi.org/10.1016/j.cell.2009.01.028

Di Florio, A., G. Capurso, M. Milione, F. Panzuto, R. Geremia, G. Delle Fave, and C. Sette. 2007. Src family kinase activity regulates adhesion, spreading and migration of pancreatic endocrine tumour cells. *Endocr. Relat. Cancer.* 14:111–124. https://doi.org/10.1677/erc.1.01318

Donepudi, M., and M.D. Resh. 2008. c-Src trafficking and co-localization with the EGF receptor promotes EGF ligand-independent EGF receptor activation and signaling. *Cell. Signal.* 20:1359–1367. https://doi.org/10.1016/j.cellsig.2008.03.007

Ducommun, S., M. Deak, D. Sumpton, R.J. Ford, A. Núñez Galindo, M. Kussmann, B. Viollet, G.R. Steinberg, M. Foretz, L. Dayon, et al. 2015. Motif affinity and mass spectrometry proteomic approach for the discovery of cellular AMPK targets: identification of mitochondrial fission factor as a new AMPK substrate. *Cell. Signal.* 27:978–988. https://doi.org/10.1016/j.cellsig.2015.02.008

Downloaded from http://rupress.org/jcb/article-pdf/217/9/3071/1614074/jcb_201802102.pdf by guest on 08 February 2026

Elias, B.C., S. Bhattacharya, R.M. Ray, and L.R. Johnson. 2010. Polyamine-dependent activation of Rac1 is stimulated by focal adhesion-mediated Tiam1 activation. *Cell Adhes. Migr.* 4:419–430. https://doi.org/10.4161/cam.4.3.12043

Fletcher, D.A., and R.D. Mullins. 2010. Cell mechanics and the cytoskeleton. *Nature.* 463:485–492. https://doi.org/10.1038/nature08908

Frame, M.C. 2002. Src in cancer: deregulation and consequences for cell behaviour. *Biochim. Biophys. Acta.* 1602:114–130.

Fuenzalida, L.C., K.L. Keen, and E. Terasawa. 2011. Colocalization of FM1-43, Bassoon, and GnRH-1: GnRH-1 release from cell bodies and their neuroprocesses. *Endocrinology.* 152:4310–4321. https://doi.org/10.1210/en.2011-1416

Ganem, N.J., and D. Pellman. 2012. Linking abnormal mitosis to the acquisition of DNA damage. *J. Cell Biol.* 199:871–881. https://doi.org/10.1083/jcb.201210040

Geiger, B., J.P. Spatz, and A.D. Bershadsky. 2009. Environmental sensing through focal adhesions. *Nat. Rev. Mol. Cell Biol.* 10:21–33. https://doi.org/10.1038/nrm2593

Goldberg, G.S., D.B. Alexander, P. Pellicena, Z.Y. Zhang, H. Tsuda, and W.T. Miller. 2003. Src phosphorylates Cas on tyrosine 253 to promote migration of transformed cells. *J. Biol. Chem.* 278:46533–46540. https://doi.org/10.1074/jbc.M307526200

He, Y., Y. Ren, B. Wu, B. Decourt, A.C. Lee, A. Taylor, and D.M. Suter. 2015. Src and cortactin promote lamellipodia protrusion and filopodia formation and stability in growth cones. *Mol. Biol. Cell.* 26:3229–3244. https://doi.org/10.1091/mbc.e15-03-0142

Hoffelder, D.R., L. Luo, N.A. Burke, S.C. Watkins, S.M. Gollin, and W.S. Saunders. 2004. Resolution of anaphase bridges in cancer cells. *Chromosoma.* 112:389–397. https://doi.org/10.1007/s00412-004-0284-6

Houk, A.R., A. Jilkine, C.O. Mejean, R. Boltyanskiy, E.R. Dufresne, S.B. Angenent, S.J. Altschuler, L.F. Wu, and O.D. Weiner. 2012. Membrane tension maintains cell polarity by confining signals to the leading edge during neutrophil migration. *Cell.* 148:175–188. https://doi.org/10.1016/j.cell.2011.10.050

Hutchins, J.R., M. Hughes, and P.R. Clarke. 2000. Substrate specificity determinants of the checkpoint protein kinase Chk1. *FEBS Lett.* 466:91–95. https://doi.org/10.1016/S0014-5793(99)01763-9

Janssen, A., M. van der Burg, K. Szuhai, G.J.P.L. Kops, and R.H. Medema. 2011. Chromosome segregation errors as a cause of DNA damage and structural chromosome aberrations. *Science.* 333:1895–1898. https://doi.org/10.1126/science.1210214

Kamranvar, S.A., D.K. Gupta, Y. Huang, R.K. Gupta, and S. Johansson. 2016. Integrin signaling via FAK-Src controls cytokinetic abscission by decelerating PLK1 degradation and subsequent recruitment of CEP55 at the midbody. *Oncotarget.* 7:30820–30830. https://doi.org/10.18632/oncotarget.9003

Kasahara, K., Y. Nakayama, Y. Nakazato, K. Ikeda, T. Kuga, and N. Yamaguchi. 2007a. Src signaling regulates completion of abscission in cytokinesis through ERK/MAPK activation at the midbody. *J. Biol. Chem.* 282:5327–5339. https://doi.org/10.1074/jbc.M608396200

Kasahara, K., Y. Nakayama, I. Sato, K. Ikeda, M. Hoshino, T. Endo, and N. Yamaguchi. 2007b. Role of Src-family kinases in formation and trafficking of macropinosomes. *J. Cell. Physiol.* 211:220–232. https://doi.org/10.1002/jcp.20931

Keller, A., A.I. Nesvizhskii, E. Kolker, and R. Aebersold. 2002. Empirical statistical model to estimate the accuracy of peptide identifications made by MS/MS and database search. *Anal. Chem.* 74:5383–5392. https://doi.org/10.1021/ac025747h

Lafaurie-Janvore, J., P. Maiuri, I. Wang, M. Pinot, J.B. Manneville, T. Betz, M. Balland, and M. Piel. 2013. ESCRT-III assembly and cytokinetic abscission are induced by tension release in the intercellular bridge. *Science.* 339:1625–1629. https://doi.org/10.1126/science.1233866

Lopez, V., N. Barinova, M. Onishi, S. Pobiega, J.R. Pringle, K. Dubrana, and S. Marcand. 2015. Cytokinesis breaks dicentric chromosomes preferentially at pericentromeric regions and telomere fusions. *Genes Dev.* 29:322–336. https://doi.org/10.1101/gad.254664.114

Maciejowski, J., Y. Li, N. Bosco, P.J. Campbell, and T. de Lange. 2015. Chromothripsis and Kataegis Induced by Telomere Crisis. *Cell.* 163:1641–1654. https://doi.org/10.1016/j.cell.2015.11.054

Mackay, D.R., and K.S. Ullman. 2015. ATR and a Chk1-Aurora B pathway coordinate postmitotic genome surveillance with cytokinetic abscission. *Mol. Biol. Cell.* 26:2217–2226. https://doi.org/10.1091/mbc.e14-11-1563

Maffei, M., M. Arbesú, A.L. Le Roux, I. Amata, S. Roche, and M. Pons. 2015. The SH3 Domain Acts as a Scaffold for the N-Terminal Intrinsically Disordered Regions of c-Src. *Structure.* 23:893–902. https://doi.org/10.1016/j.str.2015.03.009

Mishima, M., S. Kaitna, and M. Glotzer. 2002. Central spindle assembly and cytokinesis require a kinesin-like protein/RhoGAP complex with microtubule bundling activity. *Dev. Cell.* 2:41–54. https://doi.org/10.1016/S1534-5807(01)00110-1

Mitra, S.K., D.A. Hanson, and D.D. Schlaepfer. 2005. Focal adhesion kinase: in command and control of cell motility. *Nat. Rev. Mol. Cell Biol.* 6:56–68. https://doi.org/10.1038/nrm1549

Morita, E., V. Sandrin, H.Y. Chung, S.G. Morham, S.P. Gygi, C.K. Rodesch, and W.I. Sundquist. 2007. Human ESCRT and ALIX proteins interact with proteins of the midbody and function in cytokinesis. *EMBO J.* 26:4215–4227. https://doi.org/10.1038/sj.emboj.7601850

Nähse, V., L. Christ, H. Stenmark, and C. Campsteijn. 2017. The Abscission Checkpoint: Making It to the Final Cut. *Trends Cell Biol.* 27:1–11. https://doi.org/10.1016/j.tcb.2016.10.001

Peddibhotla, S., M.H. Lam, M. Gonzalez-Rimbau, and J.M. Rosen. 2009. The DNA-damage effector checkpoint kinase 1 is essential for chromosome segregation and cytokinesis. *Proc. Natl. Acad. Sci. USA.* 106:5159–5164. https://doi.org/10.1073/pnas.0806671106

Pérez, Y., M. Maffei, A. Igea, I. Amata, M. Gairí, A.R. Nebreda, P. Bernadó, and M. Pons. 2013. Lipid binding by the Unique and SH3 domains of c-Src suggests a new regulatory mechanism. *Sci. Rep.* 3:1295. https://doi.org/10.1038/srep01295

Petsalaki, E., and G. Zachos. 2013. Chk1 and Mps1 jointly regulate correction of merotelic kinetochore attachments. *J. Cell Sci.* 126:1235–1246. https://doi.org/10.1242/jcs.119677

Petsalaki, E., and G. Zachos. 2016. Clks 1, 2 and 4 prevent chromatin breakage by regulating the Aurora B-dependent abscission checkpoint. *Nat. Commun.* 7:11451. https://doi.org/10.1038/ncomms11451

Petsalaki, E., T. Akoumianaki, E.J. Black, D.A. Gillespie, and G. Zachos. 2011. Phosphorylation at serine 331 is required for Aurora B activation. *J. Cell Biol.* 195:449–466. https://doi.org/10.1083/jcb.201104023

Petsalaki, E., M. Dandoulaki, N. Morrice, and G. Zachos. 2014. Chk1 protects against chromatin bridges by constitutively phosphorylating BLM serine 502 to inhibit BLM degradation. *J. Cell Sci.* 127:3902–3908. https://doi.org/10.1242/jcs.155176

Petsalaki, E., M. Dandoulaki, and G. Zachos. 2018. The ESCRT protein Chmp4c regulates mitotic spindle checkpoint signaling. *J. Cell Biol.* 217:861–876. https://doi.org/10.1083/jcb.201709005

Piwnica-Worms, H., K.B. Saunders, T.M. Roberts, A.E. Smith, and S.H. Cheng. 1987. Tyrosine phosphorylation regulates the biochemical and biological properties of pp60c-src. *Cell.* 49:75–82. https://doi.org/10.1016/0092-8674(87)90757-4

Playford, M.P., and M.D. Schaller. 2004. The interplay between Src and integrins in normal and tumor biology. *Oncogene.* 23:7928–7946. https://doi.org/10.1038/sj.onc.1208080

Robles, E., S. Woo, and T.M. Gomez. 2005. Src-dependent tyrosine phosphorylation at the tips of growth cone filopodia promotes extension. *J. Neurosci.* 25:7669–7681. https://doi.org/10.1523/JNEUROSCI.2680-05.2005

Roskoski, R. Jr. 2015. Src protein-tyrosine kinase structure, mechanism, and small molecule inhibitors. *Pharmacol. Res.* 94:9–25. https://doi.org/10.1016/j.phrs.2015.01.003

Shenoy, S., I. Chackalaparampil, S. Bagrodia, P.H. Lin, and D. Shalloway. 1992. Role of p34cdc2-mediated phosphorylations in two-step activation of pp60c-src during mitosis. *Proc. Natl. Acad. Sci. USA.* 89:7237–7241. https://doi.org/10.1073/pnas.89.15.7237

Smith, J., L.M. Tho, N. Xu, and D.A. Gillespie. 2010. The ATM-Chk2 and ATR-Chk1 pathways in DNA damage signaling and cancer. *Adv. Cancer Res.* 108:73–112. https://doi.org/10.1016/B978-0-12-380888-2.00003-0

Steigemann, P., C. Wurzenberger, M.H. Schmitz, M. Held, J. Guizetti, S. Maar, and D.W. Gerlich. 2009. Aurora B-mediated abscission checkpoint protects against tetraploidization. *Cell.* 136:473–484. https://doi.org/10.1016/j.cell.2008.12.020

Stover, D.R., J. Liebetanz, and N.B. Lydon. 1994. Cdc2-mediated modulation of pp60c-src activity. *J. Biol. Chem.* 269:26885–26889.

Takahashi, A., Y. Obata, Y. Fukumoto, Y. Nakayama, K. Kasahara, T. Kuga, Y. Higashiyama, T. Saito, K.K. Yokoyama, and N. Yamaguchi. 2009. Nuclear localization of Src-family tyrosine kinases is required for growth factor-induced euchromatinization. *Exp. Cell Res.* 315:1117–1141. https://doi.org/10.1016/j.yexcr.2009.02.010

Tehrani, S., N. Tomasevic, S. Weed, R. Sakowicz, and J.A. Cooper. 2007. Src phosphorylation of cortactin enhances actin assembly. *Proc. Natl. Acad. Sci. USA.* 104:11933–11938. https://doi.org/10.1073/pnas.0701077104

Downloaded from http://rupress.org/jcb/article-pdf/217/9/3071/1614074/jcb_201802102.pdf by guest on 08 February 2026

Thoresen, S.B., C. Campsteijn, M. Vietri, K.O. Schink, K. Liestøl, J.S. Andersen, C. Raiborg, and H. Stenmark. 2014. ANCHR mediates Aurora-B-dependent abscission checkpoint control through retention of VPS4. *Nat. Cell Biol.* 16:550–560. https://doi.org/10.1038/ncb2959

Tominaga, T., E. Sahai, P. Chardin, F. McCormick, S.A. Courtneidge, and A.S. Alberts. 2000. Diaphanous-related formins bridge Rho GTPase and Src tyrosine kinase signaling. *Mol. Cell.* 5:13–25. https://doi.org/10.1016/S1097-2765(00)80399-8

Unsal-Kaçmaz, K., T.E. Mullen, W.K. Kaufmann, and A. Sancar. 2005. Coupling of human circadian and cell cycles by the timeless protein. *Mol. Cell. Biol.* 25:3109–3116. https://doi.org/10.1128/MCB.25.8.3109-3116.2005

Utani, K., Y. Kohno, A. Okamoto, and N. Shimizu. 2010. Emergence of micronuclei and their effects on the fate of cells under replication stress. *PLoS One.* 5:e10089. https://doi.org/10.1371/journal.pone.0010089

Waters, J.C. 2009. Accuracy and precision in quantitative fluorescence microscopy. *J. Cell Biol.* 185:1135–1148. https://doi.org/10.1083/jcb.200903097

Xu, W., S.C. Harrison, and M.J. Eck. 1997. Three-dimensional structure of the tyrosine kinase c-Src. *Nature.* 385:595–602. https://doi.org/10.1038/385595a0

Xu, W., A. Doshi, M. Lei, M.J. Eck, and S.C. Harrison. 1999. Crystal structures of c-Src reveal features of its autoinhibitory mechanism. *Mol. Cell.* 3:629–638. https://doi.org/10.1016/S1097-2765(00)80356-1

Zachos, G., E.J. Black, M. Walker, M.T. Scott, P. Vagnarelli, W.C. Earnshaw, and D.A. Gillespie. 2007. Chk1 is required for spindle checkpoint function. *Dev. Cell.* 12:247–260. https://doi.org/10.1016/j.devcel.2007.01.003

Zhang, Y., and T. Hunter. 2014. Roles of Chk1 in cell biology and cancer therapy. *Int. J. Cancer.* 134:1013–1023. https://doi.org/10.1002/ijc.28226

Downloaded from http://rupress.org/jcb/article-pdf/217/9/3071/1614074/jcb_201802102.pdf by guest on 08 February 2026